

# SU(2) chiral perturbation theory low-energy constants from 2+1 flavor staggered lattice simulations

Szabolcs Borsányi,<sup>1</sup> Stephan Dürr,<sup>1,2,\*</sup> Zoltán Fodor,<sup>1,2,3</sup> Stefan Krieg,<sup>1,2</sup>

Andreas Schäfer,<sup>4</sup> Enno E. Scholz,<sup>4,†</sup> and Kálmán K. Szabó<sup>1</sup>

<sup>1</sup>*Bergische Universität Wuppertal, Gaußstr. 20, D-42119 Wuppertal, Germany*

<sup>2</sup>*Jülich Supercomputing Centre, Forschungszentrum Jülich, D-52425 Jülich, Germany*

<sup>3</sup>*Institute for Theoretical Physics, Eötvös University, H-1117 Budapest, Hungary*

<sup>4</sup>*Universität Regensburg, Universitätsstr. 31, D-93053 Regensburg, Germany*

(Dated: May 4, 2012)

We extract the NLO low-energy constants  $\bar{\ell}_3$  and  $\bar{\ell}_4$  of SU(2) chiral perturbation theory, based on precise lattice data for the pion mass and decay constant on ensembles generated by the Wuppertal-Budapest collaboration for QCD thermodynamics. These ensembles feature 2+1 flavors of 2-fold stout-smearred dynamical staggered fermions combined with Symanzik glue, with pion masses varying from 135 MeV to 435 MeV, lattice scales between 0.7 GeV and 2.0 GeV, while  $m_s$  is kept fixed at its physical value. Moderate taste splittings and the scale being set through the pion decay constant allow us to restrict ourselves to the taste pseudoscalar state and to use formulae from continuum ChPT. Finally, by dropping the data points near 135 MeV from the fits, we can explore the range of pion masses that is needed in SU(2) ChPT to reliably extrapolate to the physical point.

PACS numbers: 11.15.Ha, 11.30.Rd, 12.38.Gc 12.39.Fe

---

\* E-mail: durr@itp.unibe.ch

† E-mail: enno.scholz@physik.uni-regensburg.de

## I. INTRODUCTION

One of the most fascinating aspects of QCD [1], the theory of strong interactions, is the non-analytic behavior of its Green's functions close to the chiral limit, that is with two or three quark masses taken small,  $m_q \ll \Lambda^2/B$ , where  $\Lambda \sim 1 \text{ GeV}$  is a typical hadronic scale and  $B$  is a condensate parameter which we will define (and determine) below.

The structure of these non-analytic contributions can be worked out in the effective field theory approach which, for the case at hand, is known as chiral perturbation theory (ChPT) [2, 3]. In this setup physical quantities are expanded in powers of  $p/\Lambda$ , where  $p$  is an external momentum, and the quark mass is treated as  $m_q \simeq O(p^2)$ . Depending on whether this is done for the two ( $u, d$ ) or three ( $u, d, s$ ) lightest flavors, the framework is known as SU(2) or SU(3) ChPT.

In either case, at the leading order of the chiral expansion there are two low-energy constants, defined from the pion decay constant as

$$F = \lim_{m_u, m_d \rightarrow 0} F_\pi, \quad B = \lim_{m_u, m_d \rightarrow 0} \{-\langle 0|\bar{q}q|0\rangle/F_\pi\} \quad (1)$$

where  $q$  denotes one of the light flavors (i.e.  $q=u$  or  $q=d$ ) in the SU(2) case, and similarly (with also  $m_s$  sent to 0) in the SU(3) case. At the next-to-leading (NLO) order, i.e. at  $O(p^4)$  in the chiral counting, 7 new low-energy constants show up in the SU(2) framework, or 10 low-energy plus 2 high-energy constants in the SU(3) framework. These low-energy constants parametrize the above mentioned chiral logarithms in the Green's functions of QCD. Their numerical values can be determined either from experiment or from an ab-initio solution of QCD in the relevant (small coupling and light quark mass) regime, as is provided by lattice QCD [4–6]. Since the chiral logarithms show up as rather subtle effects, meaningful results can only be obtained from lattice data which have excellent statistical precision and explore, at the same time, a wide enough range of lattice spacings, quark masses and box volumes such that all sources of systematic error can be controlled and eventually removed.

In this paper we provide such a determination of the SU(2) low-energy constants  $\bar{\ell}_3$  and  $\bar{\ell}_4$ . Their numerical values are extracted from the quark mass dependence of  $M_\pi$  and  $F_\pi$ , respectively, and complemented by numerical values of the leading order low-energy constants  $F$  and  $B$ . We use staggered fermion simulations with  $N_f = 2+1$  dynamical flavors, that is two degenerate light quarks of variable mass  $m_l$ , and an active strange quark

whose mass  $m_s$  is pinned down at its physical value. As a result of this our values of the low-energy constants are supposed to coincide with those in the real world. A preliminary account of our work (based on a smaller dataset) was given in [7].

The remainder of this paper is structured as follows. In Section II we specify the gauge and fermion actions used and list the ensembles which go into the determination of the chiral low-energy constants. Furthermore, details are given how we calculate the pion mass and decay constant, and how we correct the latter for the effect of the finite spatial volume of the box (which is always a small correction, since our data satisfy  $3.3 \leq M_\pi L \leq 6.8$ ). In Section III we specify the procedure through which we set, for each bare coupling  $\beta = 6/g_0^2$ , the lattice spacing  $a$  and the physical values of the bare quark masses  $m_l = (m_u + m_d)/2$  and  $m_s$ . Section IV contains the core part of the present investigation, an analysis of our data with SU(2) ChPT at NLO, with details of how we select adequate mass windows and determine the systematic uncertainty of the fitted low-energy constants. Section V contains a similar though less mature analysis at NNLO, where again the main goal is to determine the NLO coefficients, with and without the help of some priors on the remaining NLO and NNLO low-energy constants. This helps to give a reliable estimate of the theoretical uncertainty of the NLO results obtained. A summary and a comparison with the findings of other recent lattice studies of SU(2) NLO low-energy constants is presented in Section VI.

## II. LATTICE DATA

In this section we specify the lattice actions used, list the ensembles which go into the determination of the SU(2) low-energy constants, give details of how we extract the pion mass and decay constant on a given ensemble, and describe the procedure by which we remove the (small) impact of the finite spatial box size  $L$  on the data.

### A. Lattice action and ensemble generation

The lattices are generated with a tree-level Symanzik improved gauge action [8] and 2+1 flavors of staggered quarks with 2 levels of stout-smearing [9]. The action is specified in full detail in Ref. [10]. The algorithm used is a combination of HMC and RHMC with standard improvements (see e.g. [11] for an overview). Some ensembles were generated for scale

setting purposes in previous finite temperature studies [10, 12–16], and some were generated specifically for the present investigation.

We adopt a mass independent scale setting, that is the lattice spacing  $a$  depends only on the coupling  $\beta$  in the gauge action, not on the quark masses  $m_l, m_s$ . With this choice it is straightforward to adjust, for each  $\beta$ , the strange quark mass roughly to its physical value by tuning the ratio  $M_{\bar{s}s}/M_\phi$  to its physical value, where  $M_{\bar{s}s}^2 \equiv 2M_K^2 - M_\pi^2$  and  $M_\phi$  is measured from the connected contribution. Starting from the symmetric point  $m_l = m_s = m_s^{\text{phys}}$ , one can lower the light quark mass  $m_l$ , at fixed  $m_s$ , until the ratio  $M_\pi/M_{\bar{s}s}$  assumes its physical value. This is one possible definition of the physical point; other definitions differ from this one just in the choice of which ratios are affected by cut-off effects and which are not (the latter are those which are used in the definition of the physical point).

From a more practical point of view it suffices to say that we simulate, for each  $\beta$ , a number of  $(m_l, m_s)$  combinations, where  $m_s$  is held fixed and is close to whichever definition of the physical strange quark mass that one may adopt, while  $m_l$  varies between roughly the physical light quark mass and 4 to 10 times this value (depending on  $\beta$ ). The precise value of  $m_l^{\text{phys}}$  is determined, a posteriori, by means of an interpolation, as described in Section III below. A summary of our ensembles and their bare parameters is given in Table I.

## B. Calculating meson masses and decay constants

A specific advantage of staggered fermions (or of any other discretization with some form of chiral symmetry) is that the decay constant  $f = \sqrt{2}F$  of a pseudoscalar meson (in the following we will distinguish the two normalizations by using either the upper-case or the lower-case symbol) to the zero component of an axial current can be extracted without recurrence to any lattice-to-continuum matching factor.

We start from the two-point function  $C_{PP}(t)$  between two point-like pseudoscalar density operators (at least one of which is projected to zero spatial momentum) which, for an intermediate window of the Euclidean time  $t$ , takes the form

$$C_{PP}(t) = A_{PP} \left[ \exp(-Mt) + \exp(-M(T-t)) \right] \quad (2)$$

with  $T$  the lattice extent in the fourth direction. The mass  $M$  corresponds to the mass of the lightest asymptotic state with the right quantum numbers (here  $\pi$  or  $K$ ), whereas the

$\beta$	$L^3 \times T$	$am_l$	$am_s$	$\beta$	$L^3 \times T$	$am_l$	$am_s$
3.45	$24^3 \times 32$	0.0057619	0.1573	3.75	$48^3 \times 96$	0.00172000	0.048
	$16^3 \times 32$	0.0172857			$40^3 \times 64$	0.00240000	
	$12^3 \times 28$	0.0288095			$32^3 \times 64$	0.00342857	
	$12^3 \times 28$	0.0403333			$40^3 \times 64$	0.00480000	
	$12^3 \times 28$	0.0518571			$32^3 \times 64$	0.00685000	
3.55	$24^3 \times 32$	0.00374878	0.1023417	3.792	$48^3 \times 64$	0.00160714	0.045
	$16^3 \times 32$	0.01312073			$40^3 \times 64$	0.00225000	
	$16^3 \times 32$	0.01874390			$40^3 \times 64$	0.00321429	
	$12^3 \times 28$	0.02624146			$40^3 \times 64$	0.00450000	
	$12^3 \times 28$	0.03373902			$32^3 \times 64$	0.00674300	
3.67	$32^3 \times 48$	0.00231904	0.06330976	3.85	$48^3 \times 64$	0.00144606	0.0394774
	$24^3 \times 32$	0.00927616			$40^3 \times 64$	0.00197387	
	$16^3 \times 32$	0.01391424			$40^3 \times 64$	0.00281981	
	$16^3 \times 32$	0.01739280			$48^3 \times 64$	0.00394774	
	$14^3 \times 32$	0.02203088			$32^3 \times 48$	0.00578424	
					$32^3 \times 48$	0.00867636	
					$24^3 \times 48$	0.01156848	
					$24^3 \times 48$	0.01446060	

TABLE I. Overview of the staggered 2+1 flavor ensembles used in this work.

amplitude  $A_{PP}$  is proportional to the squared matrix element, i.e.  $A_{PP} \propto \langle 0|P|xy\rangle^2/M$ , where  $|xy\rangle$  denotes the pseudoscalar state put together from flavors  $x, y$  (here  $x, y = l, s$ ).

In practice it means that we determine, in a first step, the mass and the amplitude from the  $PP$  correlator. We do this either via the effective mass and amplitude method where the determination of

$$M_{\text{eff}}(t) = \frac{1}{2} \log \left( \frac{C(t-1) + \sqrt{C(t-1)^2 - C(T/2)^2}}{C(t+1) + \sqrt{C(t+1)^2 - C(T/2)^2}} \right) \quad (3)$$

$$A_{\text{eff}}(t) = \frac{C(t)}{\exp[-M_{\text{eff}}(t) t] + \exp[-M_{\text{eff}}(t) (T-t)]} \quad (4)$$

is followed by a fit to a constant over some time region  $t \in [t_{\min} : t_{\max}]$ , or using a direct fit

of the correlator to the functional form (2). In either case the data are symmetrized about  $T/2$ , and  $t_{\max} \leq T/2$ .

The decay constant is defined as  $f_{xy} = \langle 0|A_4|xy\rangle/M_{xy}$ , and via the PCAC relation this is transformed into

$$f_{xy} = (m_x + m_y) \frac{\langle 0|P|xy\rangle}{\sqrt{2}M_{xy}^2} \quad (5)$$

where  $m_{x,y}$  denotes the quark mass of the flavor  $x$  or  $y$ . Putting things together, it follows that the decay constant may be obtained from the amplitude and the mass as

$$f_{xy} \propto (m_x + m_y) \sqrt{\frac{A_{xy}}{M_{xy}^3}} \quad (6)$$

where the missing prefactors (e.g.  $L^3$ ) reflect normalization conventions which depend on the geometry, but not on the quark masses.

For the interim step, i.e. the determination of  $M_{\text{eff}}, A_{\text{eff}}$  from the correlators, a typical plateau is shown in Fig. 1. A careful look reveals some zig-zag of the data close to the mid-time point  $T/2$ . This is commonly attributed to a back-propagating parity partner [17] and reflects an effect which is specific to the staggered discretization. An advantage of the symmetric definition of the effective mass (3) is that  $M_{\text{eff}}(t)$  for an odd value of  $t$  uses only data from the original correlator at even  $t$  and vice versa. Accordingly, we can compare the results of (i) a plateau average of  $M_{\text{eff}}(t)$  for odd  $t$ , (ii) a plateau average of  $M_{\text{eff}}(t)$  for even  $t$ , and (iii) the result of a direct fit to the ansatz (2) [which does not distinguish between even and odd timeslices]. We have carefully analyzed the impact of these options and found them completely insignificant compared to both the statistical uncertainty and (even more so) the theoretical uncertainty inherent in the precise choice of the masses and lattice spacings included in the chiral fit. The latter represent relevant options that will be discussed in detail in Sections IV and V below.

### C. Finite volume corrections

Pseudoscalar masses and decay constants experience a systematic shift due to the finite spatial box length  $L$ . Approximate 3-loop and 2-loop expressions have been given for the ratios  $M_\pi(L)/M_\pi(\infty)$  and  $f_\pi(L)/f_\pi(\infty)$ , respectively, in Ref. [18]. For the range of quark masses used in this work they are supposed to give a reliable estimate of these (small) shifts.

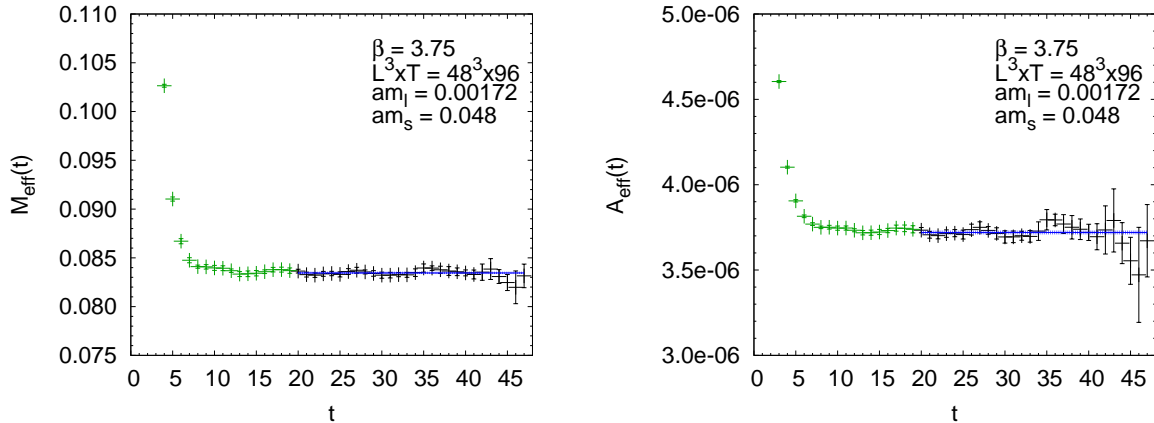


FIG. 1. Effective masses (*left panel*) and amplitudes (*right panel*) from the pion correlator at  $\beta = 3.75$ ,  $am_l = 0.00172$ ,  $am_s = 0.048$ , including the plateau-fits (*blue lines*).

The numerical values thus obtained vary between 0.1 and 2.7 per-mille for the pion mass, and between 0.2 and 7.5 per-mille for the pion decay constant. For each ensemble we thus calculate these ratios and apply them to our data. In the following, only the finite-volume corrected data are used.

### III. DETERMINING THE LATTICE SCALE AND PHYSICAL QUARK MASS

As indicated in the previous section, we wish to determine for each  $\beta$  the lattice spacing  $a$  and the physical value of  $am_l$ . Since the simulation points for one  $\beta$  are at a fixed value of  $am_s$  (which is tuned to its physical value, see Sec. II A), it is clear that the observables to be used shall include only the light but not the strange flavor, and the obvious choice is thus  $f_\pi = \sqrt{2}F_\pi$  and  $M_\pi$ .

On a more technical level we proceed by means of a two step procedure. First, we extrapolate the ratio  $(aM_l)^2/(af_l)^2 = (aM_\pi)^2/(af_\pi)^2$  of the squared pion mass and decay constant to its physical value, 1.06846. Here we use the isospin averaged and electromagnetically corrected pion mass  $M_\pi^{\text{phys}} = 134.8 \text{ MeV}$  from FLAG [19], and the PDG value of the pion decay constant  $f_\pi^{\text{phys}} = 130.41 \text{ MeV}$  [20]. In this step the purpose of the square is to reduce the amount of curvature, and we interpolate the data by means of a low-order polynomial and rational ansatz (typically with 3 parameters applied to the 5 lightest data points, i.e. with 2 degrees of freedom). We stress that the point where this ratio assumes

the desired value, 1.06846, is always very close to the lightest simulated quark mass. In view of this it should not come as a surprise that the values of  $am_l^{\text{phys}}$  that stem from the polynomial and the rational fit are always very close to each other (on the scale set by the statistical error). We use the average of the two as our central value; the difference should be seen as indicative of the systematic uncertainty of  $am_l^{\text{phys}}$  from this set of ensembles.

In the second step we consider  $af_\pi$  as a function of  $am_l$ . Again, we interpolate the data with the same polynomial and rational ansatz, and determine the ordinate value at the abscissa point that was specified in the previous step. This value  $af_\pi$  is then identified with the product of the lattice spacing  $a$  and the PDG value  $f_\pi^{\text{phys}} = 130.41$  MeV [20]; this yields the lattice spacing  $a$  in fm for the lattice theory at that particular value of the coupling  $\beta$ . A typical example of this two-step procedure is shown in Fig. 2; in the relevant range (close to the lightest mass point) the difference between the two ansätze is invisibly small. Furthermore, in Tab. II the results for the physical light quark masses and lattice spacings obtained by this method are displayed.

As a final comment, let us remark that already in these two steps one could, in principle, use ChPT. We rather prefer to stay with the simple yet robust procedure as sketched above. It makes it apparent that some of the chiral fits (with an inappropriate fitting window) going wild (as will be discussed in Sections IV and V below) is not linked to a potential mishap in the physical mass and scale determination. In other words, we take the lattice spacing and the physical light quark mass from an “ideal” simulation where  $M_\pi/f_\pi$  is exactly tuned to its physical value, and use this knowledge regardless of how many data-points enter the chiral fits described below. Needless to comment that for those NLO and NNLO fits which work fine (and which include the lightest data points), their intrinsic physical mass and scale determination was always found to be in very good agreement with the result of the procedure described in the previous two paragraphs.

#### IV. FITS TO NLO-SU(2) CHPT

In this section we will describe how we fit the mass dependence of the meson decay constant and its squared mass to the prediction of next-to-leading order (NLO) ChPT and in this way obtain the low-energy constants (LECs) appearing in these ChPT-formulae. Since in the simulations considered here the strange quark mass was fixed to its physical



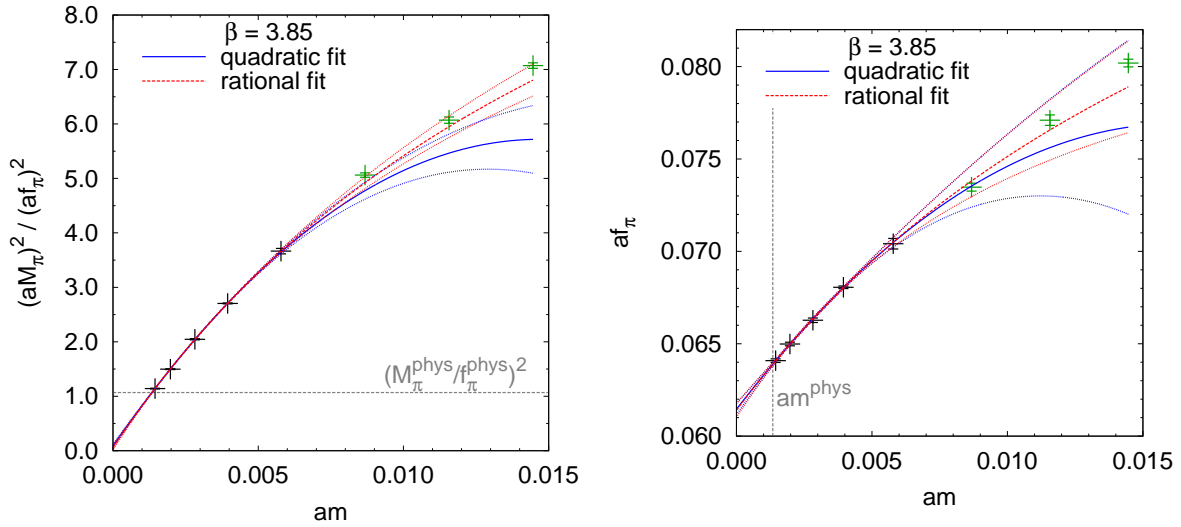


FIG. 2. Fits to the ratio  $(aM_\pi)^2/(af_\pi)^2$  (left panel) and the decay constant  $af_\pi$  (right panel) at  $\beta = 3.85$  to obtain the physical light quark mass  $am^{\text{phys}}$  and the lattice scale  $1/a$ . Shown are quadratic (solid blue lines) and rational (dashed red lines) fits including the black data points, green data points were excluded from the fits. Error bands are shown by dotted lines. The dashed grey lines mark the value of the ratio at the physical point and the physical light quark mass extracted therefrom.

$\beta$	$am^{\text{phys}}$	$1/a / \text{GeV}$	$a / \text{fm}$
3.45	$5.771(18) \cdot 10^{-3}$	0.69468(67)	0.28406(27)
3.55	$3.612(18) \cdot 10^{-3}$	0.9165(12)	0.21531(28)
3.67	$2.191(15) \cdot 10^{-3}$	1.3063(25)	0.15105(29)
3.75	$1.6889(55) \cdot 10^{-3}$	1.6288(15)	0.12115(11)
3.792	$1.5355(70) \cdot 10^{-3}$	1.7935(22)	0.11002(14)
3.85	$1.3430(98) \cdot 10^{-3}$	2.0410(35)	0.09668(16)

TABLE II. Physical light quark mass  $am^{\text{phys}}$ , lattice scale  $1/a$  and spacing  $a$  at different  $\beta$  obtained by the method described in Sec. III.

value, we will only deal with the light quark mass dependence described by SU(2) ChPT. The LECs extracted in this way therefore contain the correct contribution of the effects due to the strange quark present in nature. Further, we are restricting ourselves to the case of a degenerate light quark mass, which we will denote by  $m$  (or  $am$  in lattice units) throughout the remainder of this paper, i.e., from now on we drop the subscript  $l$  on the light quark mass parameter. At the physical point, this mass corresponds to the average mass of the two light quarks observed in nature:  $m^{\text{phys}} = (m_u^{\text{phys}} + m_d^{\text{phys}})/2$ .

In the following we will try to fit our data to continuum ChPT and not consider variants of ChPT, which take into account lattice discretization effects and/or taste violations present in the staggered formulation, see e.g. [17, 21, 22]. Whether a continuum ansatz is suitable to describe our data is not a priori clear and needs to be tested. It is valid if, within the statistical precision of our data, no cut-off dependence is seen in the observables considered. As will be shown below, this is indeed the case for our  $M_\pi$  and  $f_\pi$  data in the relevant region. This can be traced back to the combined effect of (a) the two levels of stout smearing in the action (see Sec. II) and (b) the specific choice of our scaling trajectory, i.e. the scale and the physical quark mass being set through  $f_\pi$  and  $M_\pi$  (see Sec. III). While (b) ensures that discretization effects on both  $M_\pi$  and  $f_\pi$  vanish at the physical point, (a) keeps them small in its vicinity due to the suppression of taste violations (see e.g. [23, 24] and [15]). As we will see below, the combination of these two effects leads to a suppression of discretization effects within our statistical precision over a sufficiently wide region of quark masses and lattice spacings.

### A. Methods and fit formulae

ChPT up to NLO predicts for the decay constant  $f_\pi$  and the squared mass  $M_\pi^2$  of a meson consisting of two mass-degenerate quarks of mass  $m$  the following functional form [2, 3, 19]

$$M_\pi^2 = \chi \left[ 1 + \frac{\chi}{16\pi^2 f^2} \log \frac{\chi}{\Lambda_3^2} \right], \quad (7)$$

$$f_\pi = f \left[ 1 - \frac{\chi}{8\pi^2 f^2} \log \frac{\chi}{\Lambda_4^2} \right], \quad (8)$$

$$\chi = 2Bm. \quad (9)$$

At this order four LECs appear: the decay constant  $f$  in the SU(2)-chiral limit ( $m \rightarrow 0$ ), the mass-parameter  $B$  and two low-energy scales  $\Lambda_3$  and  $\Lambda_4$ . The mass parameter  $B$  depends like

the quark mass itself on the renormalization scheme but the combination  $\chi$  of this parameter and the quark mass are renormalization scheme-independent and it is this combination which will be used exclusively in this work. The low-energy scales are related to the LECs  $\bar{\ell}_3$  and  $\bar{\ell}_4$  at the scale of the physical pion mass  $M_\pi^{\text{phys}}$  via

$$\bar{\ell}_i = \log \frac{\Lambda_i^2}{(M_\pi^{\text{phys}})^2}, \quad i = 3, 4. \quad (10)$$

Since we used the physical values  $f_\pi^{\text{phys}}$  and  $(M_\pi^{\text{phys}})^2$  to set the scale and determine the physical light quark mass  $m^{\text{phys}}$  for each set of lattice ensembles with a given gauge coupling  $\beta$ , our ansatz should reproduce the physical point. Note also, that each set of lattice ensembles contained one simulated point in close vicinity of the physical point. Therefore, we could impose the following constraints to the chiral formulae (Eqs. (7, 8))

$$M_\pi^2|_{m=m^{\text{phys}}} = (M_\pi^{\text{phys}})^2, \quad f_\pi|_{m=m^{\text{phys}}} = f_\pi^{\text{phys}}. \quad (11)$$

As it is easily derived, these two constraints result in the relations

$$\log \frac{\chi^{\text{phys}}}{\Lambda_3^2} = \frac{16\pi^2 f^2}{(\chi^{\text{phys}})^2} \left( (M_\pi^{\text{phys}})^2 - \chi^{\text{phys}} \right), \quad (12)$$

$$\log \frac{\chi^{\text{phys}}}{\Lambda_4^2} = \frac{8\pi^2 f^2}{f_\pi^{\text{phys}}} \left( f - f_\pi^{\text{phys}} \right) \quad (13)$$

between the LECs, where  $\chi^{\text{phys}} = 2Bm^{\text{phys}}$ . Using them to eliminate, e.g., the low-energy scales from the NLO ChPT formulae, the constrained formulae can be written as

$$M_\pi^2 = \chi \left[ 1 + \frac{\chi}{16\pi^2 f^2} \log \frac{\chi}{\chi^{\text{phys}}} + \frac{\chi}{\chi^{\text{phys}}} \frac{(M_\pi^{\text{phys}})^2 - \chi^{\text{phys}}}{\chi^{\text{phys}}} \right], \quad (14)$$

$$f_\pi = f \left[ 1 - \frac{\chi}{8\pi^2 f^2} \log \frac{\chi}{\chi^{\text{phys}}} - \frac{\chi}{\chi^{\text{phys}}} \frac{f - f_\pi^{\text{phys}}}{f} \right]. \quad (15)$$

Note that  $\chi/\chi^{\text{phys}} = m/m^{\text{phys}}$ . These formulae now depend on two LECs:  $B$  and  $f$ , and the two physical input values  $M_\pi^{\text{phys}}$  and  $f_\pi^{\text{phys}}$ . In our fitting procedure only  $\chi^{\text{phys}}$  and  $f$  will be treated as free parameters. For that reason, we also like to refer to these fits as parameter reduced fits. (Of course, by treating  $M_\pi^{\text{phys}}$  and  $f_\pi^{\text{phys}}$  as free parameters as well, one would recover the unconstrained Eqs. (7, 8), respectively.)

In the following, we want to perform combined (i.e., fitting  $M_\pi^2$  and  $f_\pi$  simultaneously) global fits to our lattice data at the different gauge couplings available to us. For this reason we make use of the lattice scale and physical light quark mass determined beforehand (see

Sec. III). The meson mass and decay constant in lattice units at a given gauge coupling  $\beta$  are converted into physical units by

$$M_\pi^2 = (1/a)_\beta^2 (aM_\pi)_\beta^2, \quad f_\pi = (1/a)_\beta (af_\pi)_\beta,$$

respectively. Furthermore, we rewrite the combination  $\chi = 2Bm$  as

$$\chi = (2Bm^{\text{phys}}) \frac{(am)_\beta}{(am^{\text{phys}})_\beta} = \chi^{\text{phys}} \frac{(am)_\beta}{(am^{\text{phys}})_\beta}$$

and will determine only the renormalization-independent combination  $\chi^{\text{phys}} = 2Bm^{\text{phys}}$  in our fits. The factor  $m^{\text{phys}}$  will be removed, based on external data, in Sec. VI.

## B. Combined global fits

### 1. NLO-ChPT without constraints

We begin the discussion of the chiral fits with the results of applying the unconstrained fit formulae, Eqs. (7, 8), to our data. The combined fit has four free parameters:  $\chi^{\text{phys}} = 2Bm^{\text{phys}}$ ,  $f$ ,  $\Lambda_3$ , and  $\Lambda_4$ . A priori, it is not clear whether all simulated lattice spacings will lie in the scaling region, especially for the very coarse lattices with lattice spacings of up to 0.28 fm (corresponding to a lattice scale of  $1/a \approx 0.7$  GeV) this is questionable. Also, the range of quark masses or equivalently meson masses to which NLO-SU(2) ChPT is applicable will have to be determined. Eventually, the fit quality, which we measure by the standard  $\chi^2/\text{d.o.f.}$ , will be used to decide on these issues. In Fig. 3 we provide a landscape of the simulated meson masses at the various lattice spacings. The horizontal dashed lines indicate the various mass-cuts we applied in our global combined fits. One should keep in mind, that for the combined fit each point in the landscape plot represents two data points: one for the meson mass and one for the meson decay constants.

In Fig. 4 we show the result of a combined fit to the meson masses and decay constants to the data at all available lattice spacings and a mass range of  $135 \text{ MeV} \leq M_\pi \leq 390 \text{ MeV}$ , i.e. excluding only the heaviest point at each simulated  $\beta$ -value. These plots show all available data points, whether or not included in the fit range. We marked those points which have been excluded by green symbols, while points included in the fit range are marked by black symbols. As one can already judge by eye, this fit gives a bad  $\chi^2/\text{d.o.f.}$  of about 4.1, although

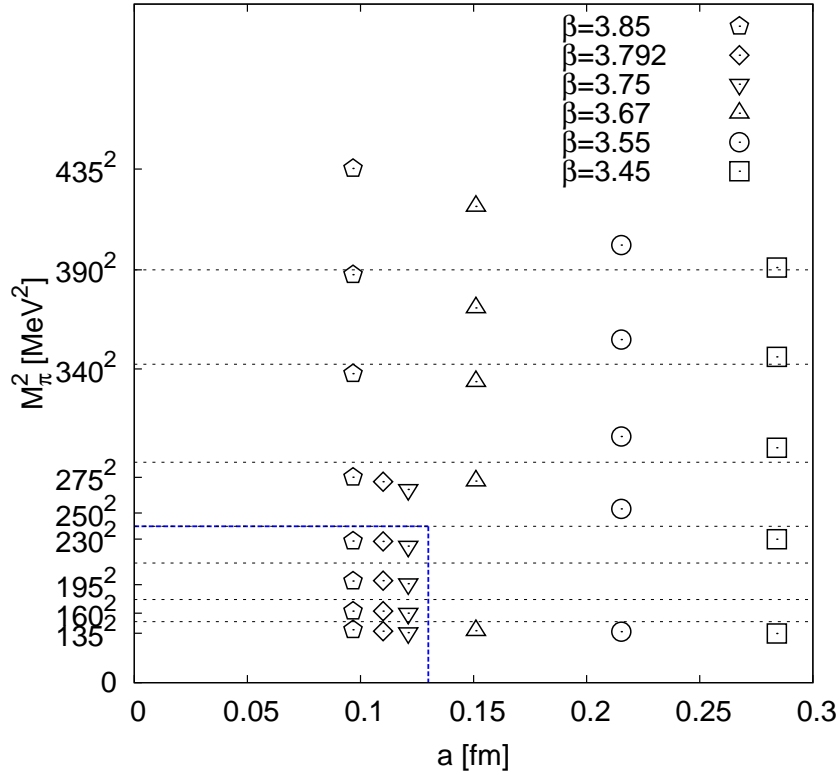


FIG. 3. Landscape plot of the simulated (squared) meson masses  $M_\pi^2$  versus the lattice spacing  $a$ . The *horizontal dashed lines* indicate the various mass cuts we apply in our chiral fits. The *blue dashed line* indicates our final preferred fit range, see text for details.

the fitted parameters are in a reasonable range, cf. Fig. 5. In a first step, we consider reducing the mass range by excluding more and more of the heavier points as indicated by the dashed horizontal lines in our landscape plot, Fig. 3. In Fig. 5 we show how the fitted parameters and the  $\chi^2/\text{d.o.f}$  vary when we change the mass range in the fit, still considering the ensembles at all available lattice spacings. First we focus on those fit ranges including the near physical points which are shown above the top-most dashed horizontal line in each of the plots in Fig. 5. (In the fit results shown below that line the near physical points and subsequently other points with light meson masses have been excluded, we will comment on those results below.) As one can see, the  $\chi^2/\text{d.o.f}$  improves by narrowing the fit range and for the range  $135 \text{ MeV} \leq M_\pi \leq 240 \text{ MeV}$  it is already comparable with 1.0. Also the four fit parameters seem to reach a plateau at this fit range. Note, that for the two narrowest fit ranges (upper

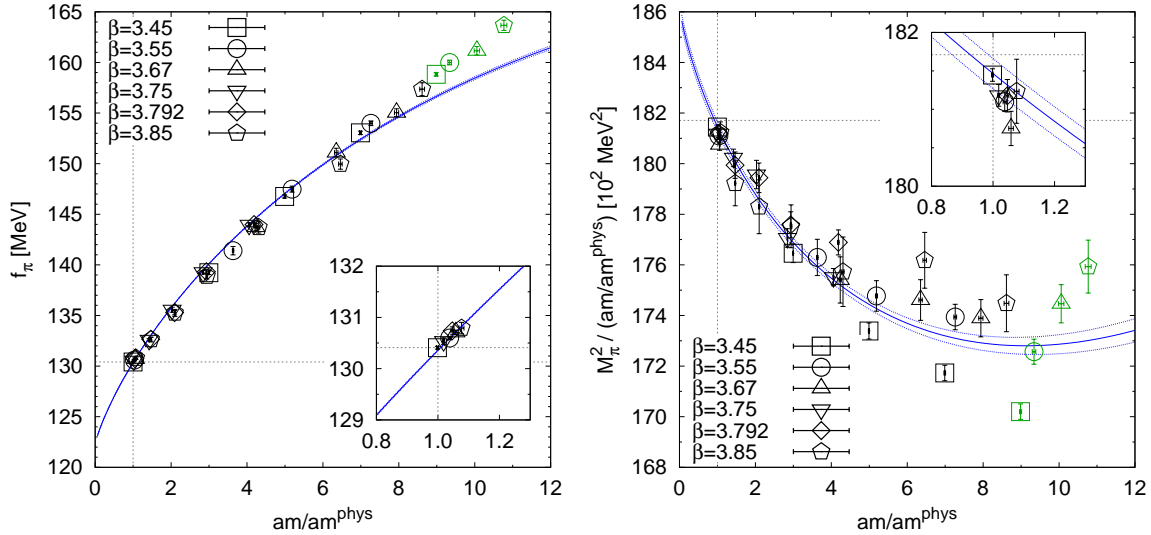


FIG. 4. Combined fit for all lattice scales,  $135 \text{ MeV} \leq M_\pi \leq 390 \text{ MeV}$ . *Left panel:* meson decay constant, *right panel:* squared meson mass divided by quark mass ratio. Points marked by *black symbols* are included in the fit, those marked by *green symbols* are excluded. The physical values are indicated by *dashed gray lines*.

mass limit at 160 or 195 MeV) the number of available data points might be too small as is also indicated by the larger error bars at these ranges. We already show in these plots the central values and error bands as determined from our preferred fit below, just to demonstrate that these error bands are compatible with the values obtained from fits to all ensembles. For completeness, in Fig. 6 we show the LECs  $\bar{\ell}_3$ ,  $\bar{\ell}_4$  and the phenomenologically relevant ratio  $f_\pi^{\text{phys}}/f$  as determined from our fits with different mass ranges.

In a second step, we will now examine whether or not all the available lattice spacings already lie in the scaling region. Remember, that since the meson mass and decay constant define our scaling trajectory, no terms modelling discretization effects have been added to our chiral formulae. To test the scaling behaviour, we excluded ensembles belonging to one or more gauge coupling  $\beta$  from the fits. In Fig. 7 we show how the fit parameters and  $\chi^2/\text{d.o.f.}$  change with respect to which lattice spacings are included in the fits. We show this for two different mass ranges, both including the near physical points. The leftmost point on each of these plots is from a fit to all available lattice spacings. Then, separated by vertical dashed lines, follow groups of fits where one, two, three or four lattice spacings have

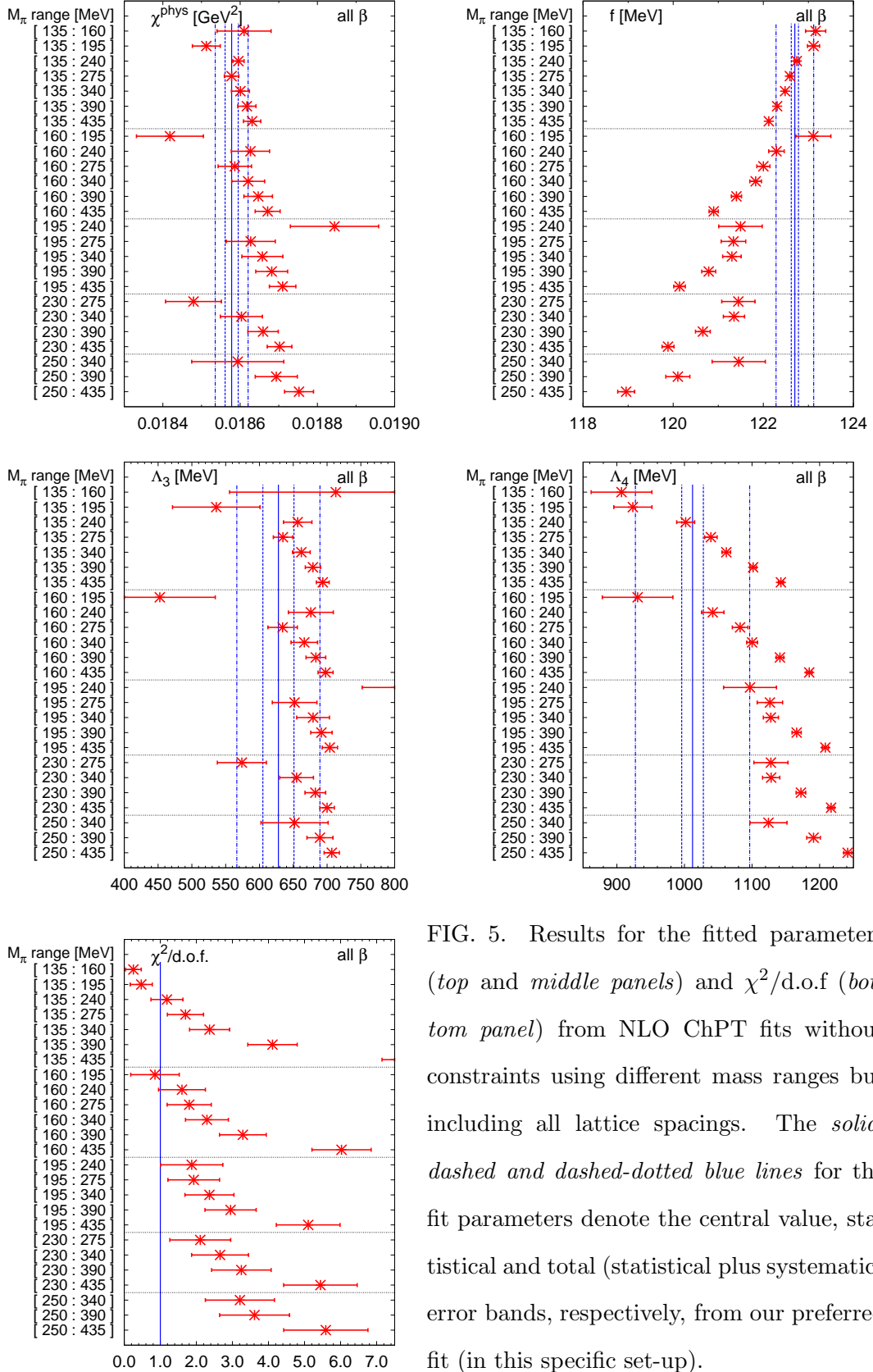


FIG. 5. Results for the fitted parameters (*top and middle panels*) and  $\chi^2/\text{d.o.f}$  (*bottom panel*) from NLO ChPT fits without constraints using different mass ranges but including all lattice spacings. The *solid, dashed and dashed-dotted blue lines* for the fit parameters denote the central value, statistical and total (statistical plus systematic) error bands, respectively, from our preferred fit (in this specific set-up).

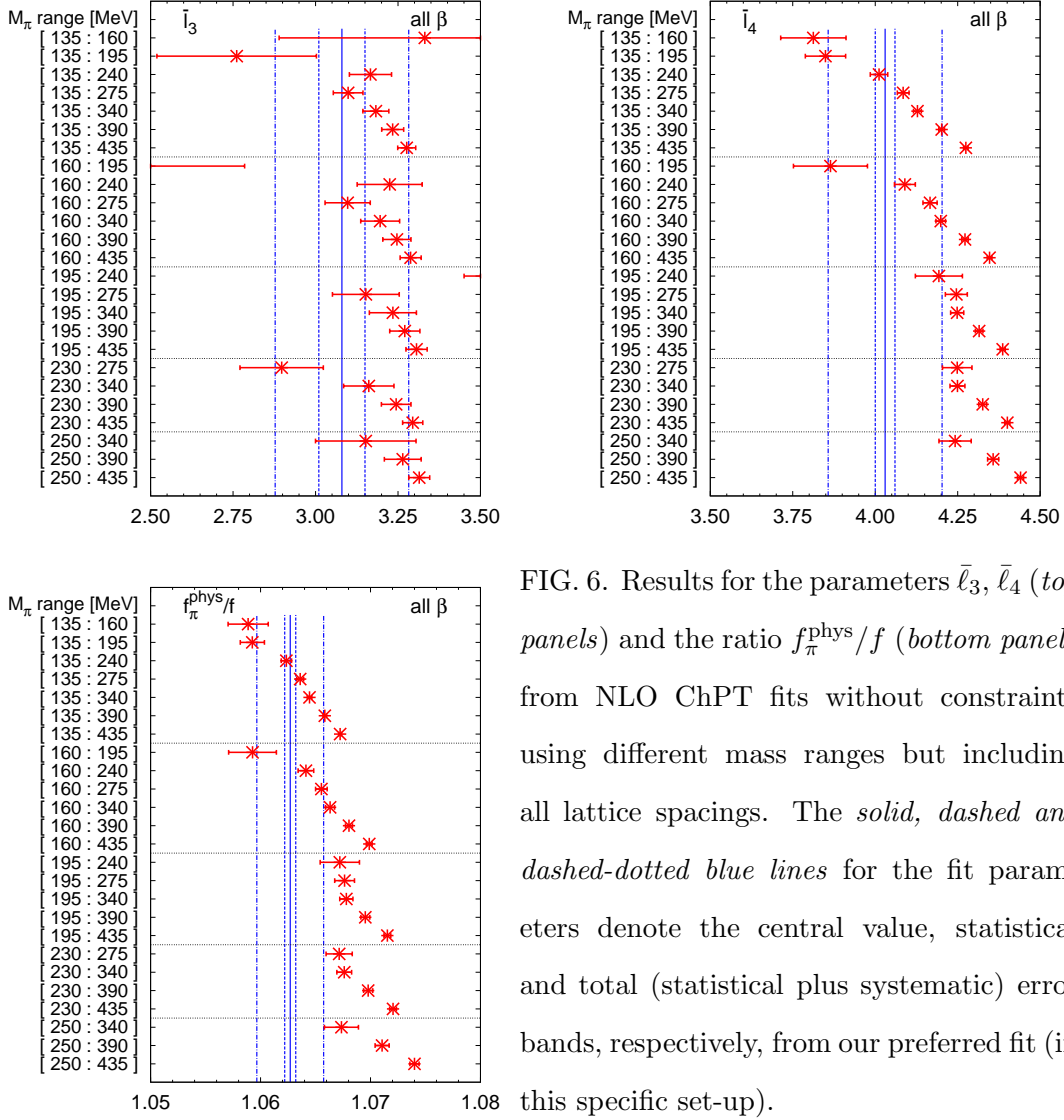


FIG. 6. Results for the parameters  $\bar{l}_3$ ,  $\bar{l}_4$  (top panels) and the ratio  $f_\pi^{\text{phys}}/f$  (bottom panel) from NLO ChPT fits without constraints using different mass ranges but including all lattice spacings. The solid, dashed and dashed-dotted blue lines for the fit parameters denote the central value, statistical and total (statistical plus systematic) error bands, respectively, from our preferred fit (in this specific set-up).

been excluded. The horizontal blue lines show our final estimate with error bands of the quantity displayed. Especially in the group where three lattice spacings have been excluded (the second from the right), we observe the parameters to reach a plateau by excluding the coarse lattice spacings. Overall, it is also reassuring that all the points fall into the error band of the combined statistical and systematic error, which we are going to discuss in the remainder now.

From the previous discussion about excluding coarser lattice spacings from the chiral analysis, we decided to restrict the range in the lattice spacings to  $1/a > 1.6 \text{ GeV}$  or  $a \leq 0.12 \text{ fm}$ , i.e., only the ensembles at gauge couplings  $\beta = 3.75, 3.792, \text{ and } 3.85$  will be included. Figures 8 and 9 show the dependence of the fitted parameters and derived



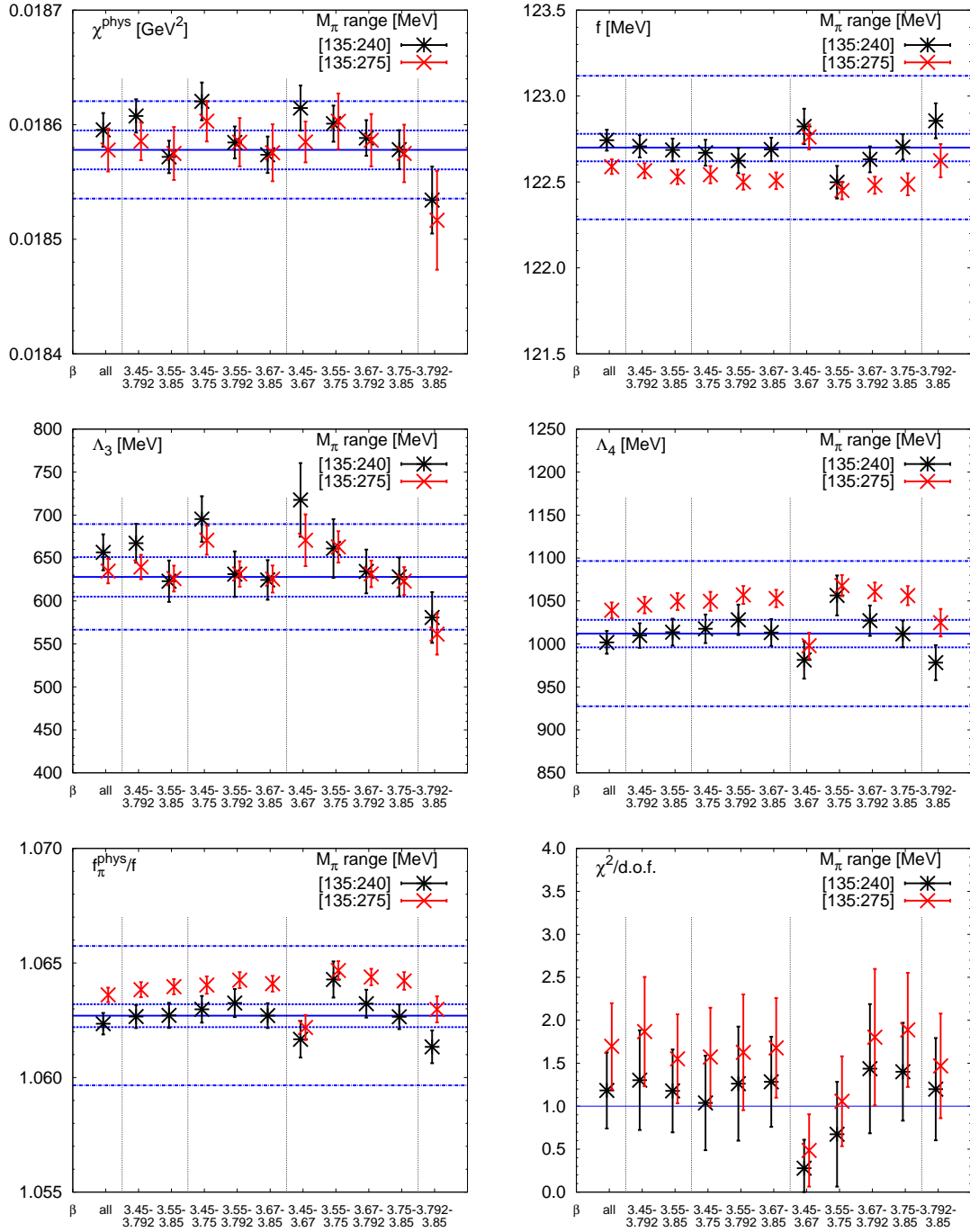


FIG. 7. Fit parameters and  $\chi^2/\text{d.o.f.}$  from NLO ChPT fits without constraints to two different mass ranges, where several lattice spacings have been excluded. *Vertical dashed lines* group points where no, one, two, three or four (from left to right) lattice spacings have been excluded. The *solid, dashed and dashed-dotted horizontal blue lines* denote the central value, statistical and total (statistical plus systematic) error bands, respectively, from our preferred fit.

quantities on the range of meson masses included in the fit range. These figures should be compared with Figs. 5 and 6. Again, we observe the same pattern of reaching plateaus when excluding more and more heavier meson masses. Eventually, we decided to take the mass range  $135 \text{ MeV} \leq M_\pi \leq 240 \text{ MeV}$  as our preferred fit, from which we will quote the central values and statistical errors. This choice is also indicated in the landscape plot, Fig. 3, by the dashed blue lines. The combined global fit has an acceptable  $\chi^2/\text{d.o.f.} = 1.4(0.6)$  and is shown in Fig. 10. In the top panels only the data points included in the fit are plotted, while the bottom panels show the excluded data points as well. To estimate the systematic error on a fitted parameter, we take the variance of this parameter with respect to the fits using different mass ranges, which also include the near physical points. These are the top-most points above the first horizontal dashed line in each panel of Figs. 8 and 9. This procedure results in the set of LECs given in the left column of Tab. III. Note, that only the first four parameters are fit parameters, while the remaining ones are subsequently derived from this set of parameters. The central values and error bands (statistical and combined statistical and systematic) have always been shown in the various compilations of fit results (Figs. 5, 6, 7, 8, 9). It is reassuring that basically all relevant results are compatible with these error bands, which a posteriori justifies our procedure of estimating the systematic error.

In the remainder of this section, we want to discuss briefly the influence of the near physical points on the fits and the results of the fitted quantities. As an example, we provide in Fig. 11 the result of a combined global fit in the mass range  $195 \text{ MeV} \leq M_\pi \leq 275 \text{ MeV}$  using ensembles with  $1/a > 1.6 \text{ GeV}$ . As can be seen from the insert magnifying the region around the physical point, for the pion decay constant the fit misses the points simulated in that region by a couple of standard deviations resulting in an extrapolated  $f_\pi^{\text{phys}} = 129.5(0.2) \text{ MeV}$  (stat. error only), which has to be compared to the value of  $130.41(0.03)(0.20)$  quoted by the PDG [20]. For the extrapolated squared pion mass the situation looks better. In Fig. 12 we provide the values for  $f_\pi^{\text{phys}}$  and  $(M_\pi^{\text{phys}})^2$  extrapolated to the physical point by our NLO-ChPT fits with various mass ranges using ensembles with  $1/a > 1.6 \text{ GeV}$  only. In these two plots, the solid and dashed blue lines represent the central value and (total) error band for these quantities as quoted by [19, 20]. As one can clearly see, while the extrapolated squared pion mass is within errors compatible with the experimental result, the extrapolated pion decay constant starts to shift towards lower values once the nearly physical points are excluded from the fit range. This shift increases with both an increasing lower and higher

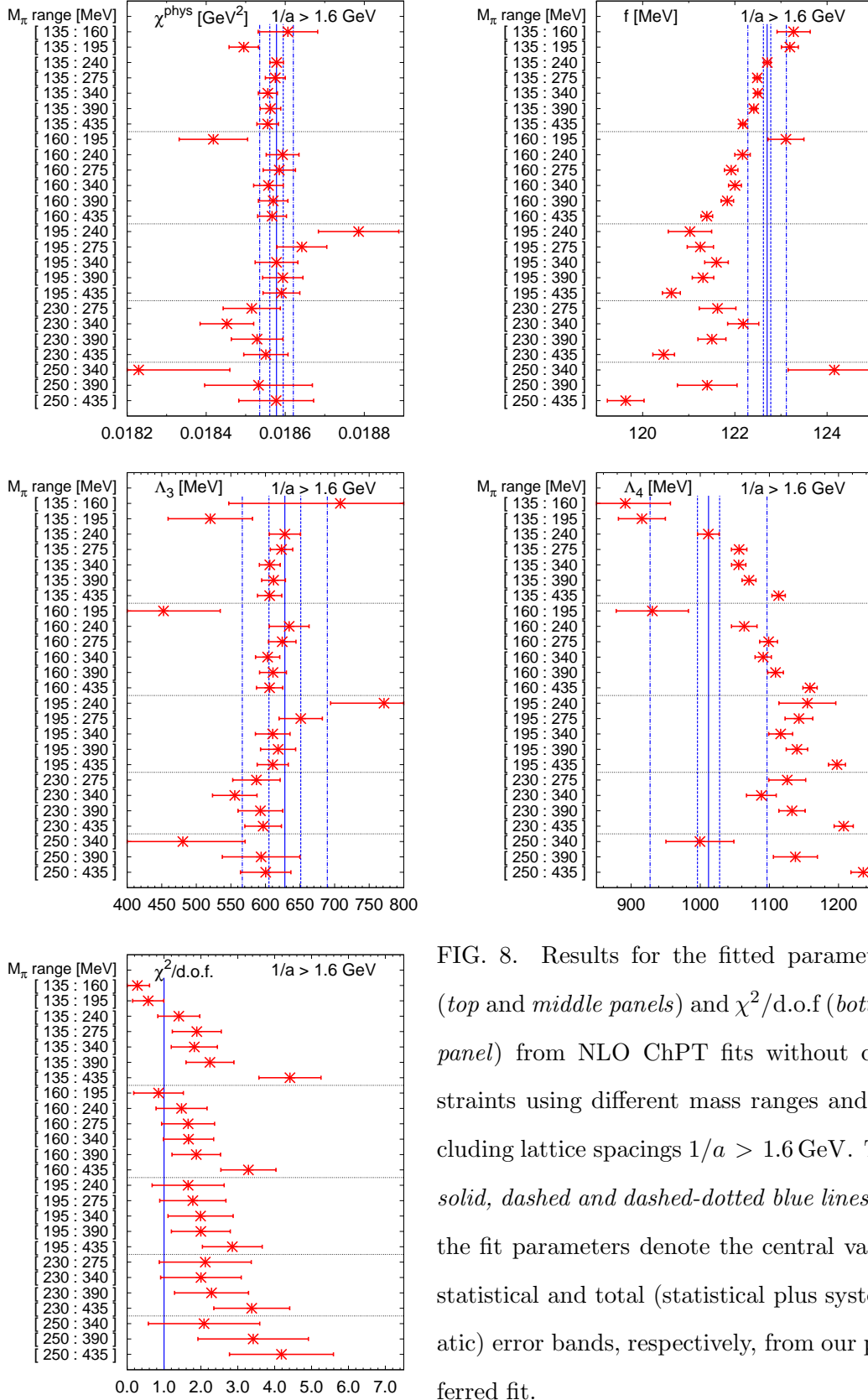


FIG. 8. Results for the fitted parameters (top and middle panels) and  $\chi^2/\text{d.o.f.}$  (bottom panel) from NLO ChPT fits without constraints using different mass ranges and including lattice spacings  $1/a > 1.6$  GeV. The solid, dashed and dashed-dotted blue lines for the fit parameters denote the central value, statistical and total (statistical plus systematic) error bands, respectively, from our preferred fit.

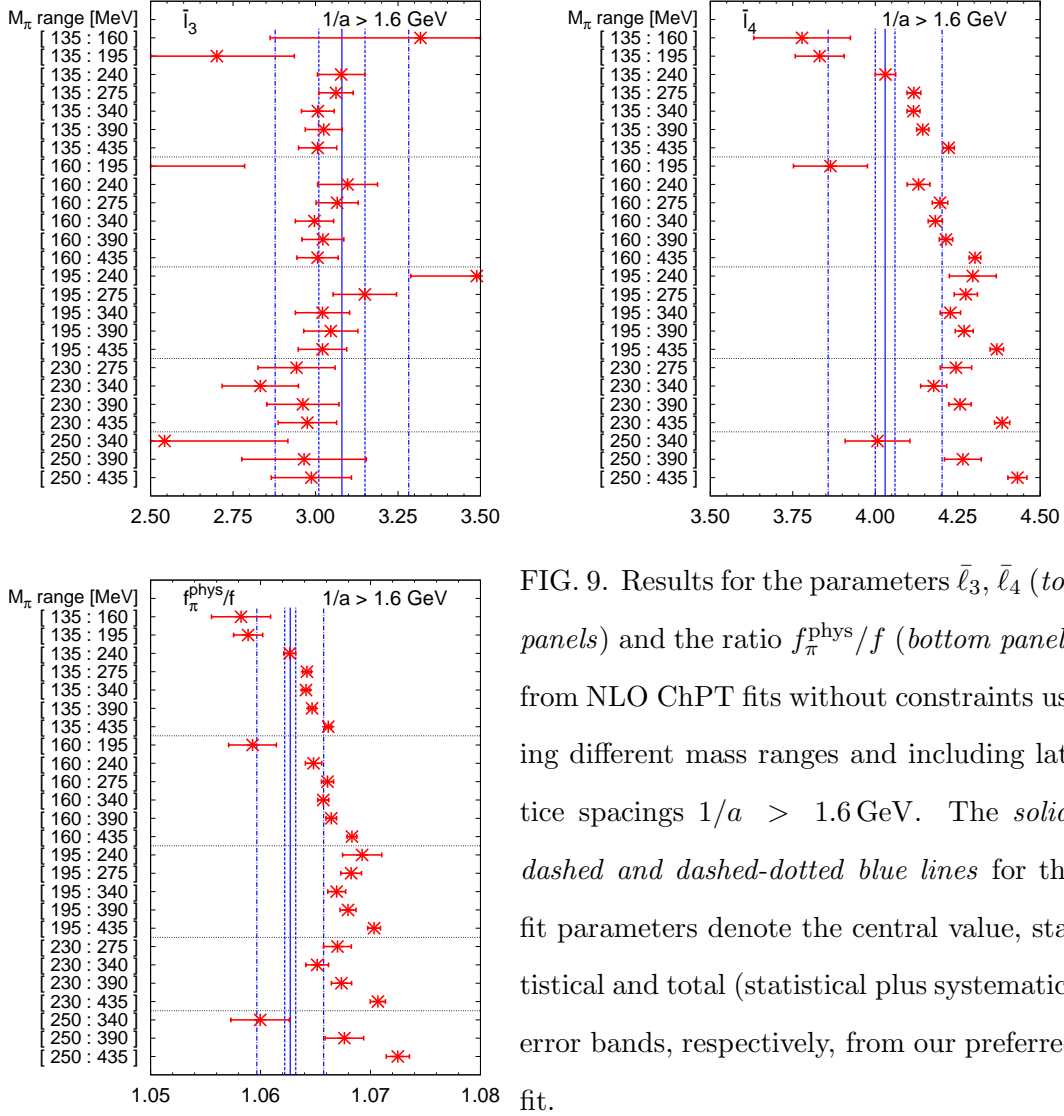


FIG. 9. Results for the parameters  $\bar{\ell}_3$ ,  $\bar{\ell}_4$  (top panels) and the ratio  $f_\pi^{\text{phys}}/f$  (bottom panel) from NLO ChPT fits without constraints using different mass ranges and including lattice spacings  $1/a > 1.6 \text{ GeV}$ . The solid, dashed and dashed-dotted blue lines for the fit parameters denote the central value, statistical and total (statistical plus systematic) error bands, respectively, from our preferred fit.

bound on the fit range as can be seen from the plot. This behaviour is also in accordance with what could be observed in the mass range plots for the fitted parameters (Figs. 5, 8) and derived phenomenological quantities (Figs. 6, 9) shown before. Whereas for quantities like  $\chi^{\text{phys}}$  and  $\Lambda_3$  (or  $\bar{\ell}_3$ ) which predominantly influence the quark mass dependence of  $M_\pi^2$ , the values from fits excluding ensembles with low meson masses are still in agreement with our estimate. This is no longer the case for the quantities  $f$  and  $\Lambda_4$  (or  $\bar{\ell}_4$ ) predominantly influencing the quark mass dependence of  $f_\pi$ . It is noteworthy though, that the ratio  $f_\pi^{\text{phys}}/f$  (where  $f_\pi^{\text{phys}}$  is the value extrapolated from the fit) as well shows a tendency to shift towards higher values once more and more lighter masses are excluded, see e.g. bottom panel of Fig. 9, although both  $f$  and  $f_\pi^{\text{phys}}$  are shifting towards lower values, see Figs. 8 and 12, re-

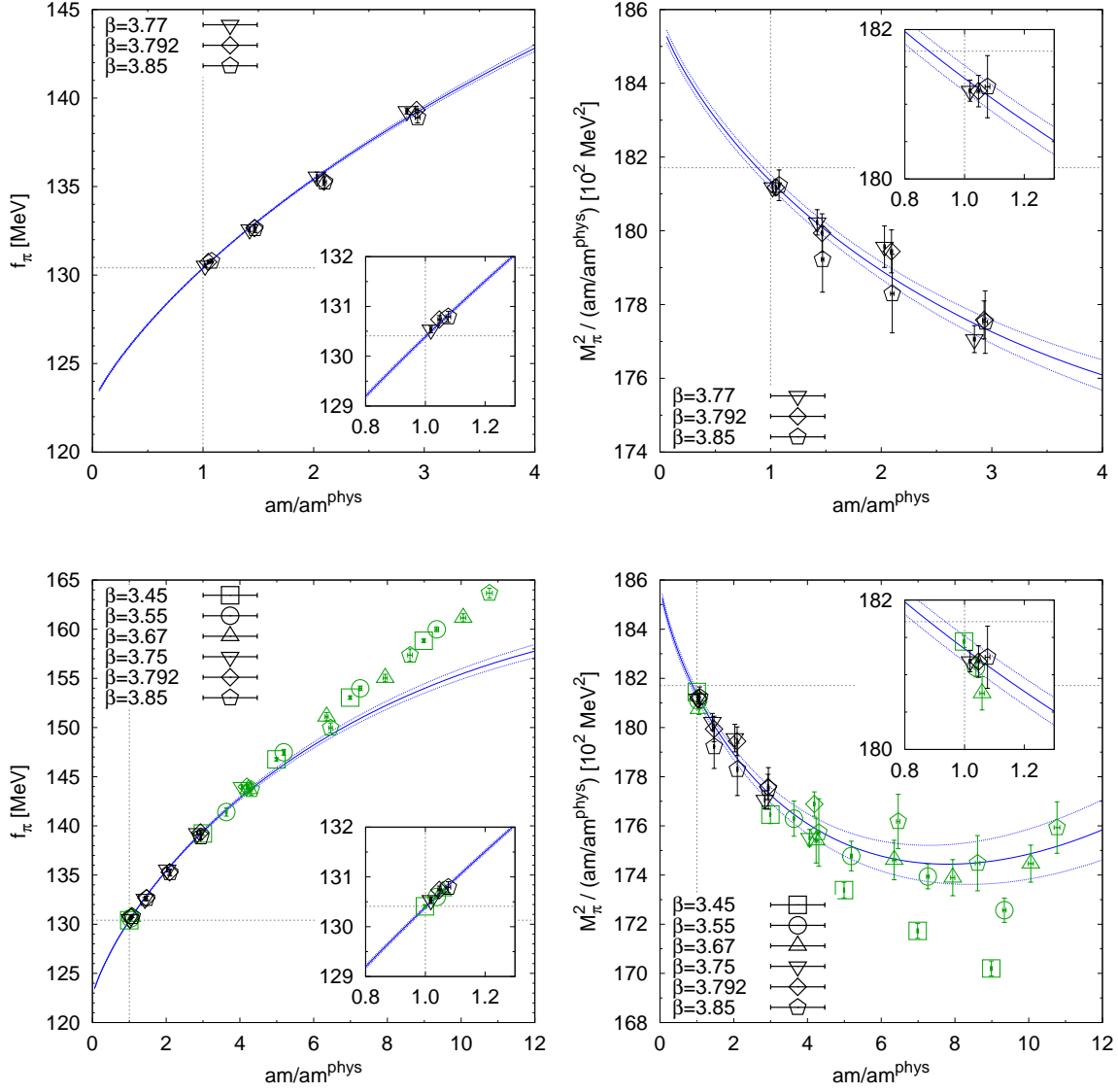


FIG. 10. Combined fit for lattice scales  $1/a > 1.6 \text{ GeV}$  and meson masses  $135 \text{ MeV} \leq M_\pi \leq 240 \text{ MeV}$ . *Left panels:* meson decay constant, *right panels:* squared meson mass divided by quark mass ratio. The *top panels* show only the points, which have been included in the fit, while the *bottom panels* show all points. There, points marked by *black symbols* are included in the fit, those marked by *green symbols* are excluded. The physical values are indicated by *dashed gray lines*.

spectively. In our opinion, the aforementioned observations show the danger when applying ChPT-formulae to (lattice) data, where the lowest pion masses are still too heavy.

	unconstrained	parameter-reduced
$\chi^{\text{phys}}/(10^{-2}\text{GeV}^2)$	1.8578(17) <sub>stat</sub> (39) <sub>syst</sub>	1.8639(18) <sub>stat</sub> (44) <sub>syst</sub>
$f/\text{MeV}$	122.70(08) <sub>stat</sub> (41) <sub>syst</sub>	122.73(06) <sub>stat</sub> (28) <sub>syst</sub>
$\Lambda_3/\text{MeV}$	628(23) <sub>stat</sub> (57) <sub>syst</sub>	678(40) <sub>stat</sub> (119) <sub>syst</sub>
$\Lambda_4/\text{MeV}$	1,012(16) <sub>stat</sub> (83) <sub>syst</sub>	1,006(15) <sub>stat</sub> (71) <sub>syst</sub>
$\bar{\ell}_3$	3.08(07) <sub>stat</sub> (19) <sub>syst</sub>	3.23(12) <sub>stat</sub> (30) <sub>syst</sub>
$\bar{\ell}_4$	4.03(03) <sub>stat</sub> (17) <sub>syst</sub>	4.02(03) <sub>stat</sub> (14) <sub>syst</sub>
$f_{\pi}^{\text{phys}}/f$	1.0627(05) <sub>stat</sub> (30) <sub>syst</sub>	1.0626(06) <sub>stat</sub> (24) <sub>syst</sub>

TABLE III. Results for LECs from unconstrained (*left column*, see Sec. IV B 1 for details) and parameter-reduced fits (*right column*, see Sec. IV B 2 for details). In case of the unconstrained fits the first four entries ( $\chi^{\text{phys}}$ ,  $f$ ,  $\Lambda_3$ ,  $\Lambda_4$ ) are free fit parameters while the remaining entries are derived from these. For the parameter-reduced fit only the first two entries ( $\chi^{\text{phys}}$ ,  $f$ ) are free fit parameters. These two sets are used to calculate the final values as quoted in Eqs. (16–22).

## 2. Parameter-reduced NLO-ChPT

As mentioned in the beginning of this section, we also considered parameter-reduced NLO-ChPT fits which are constrained to reproduce the physical values of the pion mass and decay constant at the physical quark mass, see Eqs. (14, 15). This will reduce the number of fit parameters in our combined global NLO-fits from four to two, leaving us with  $\chi^{\text{phys}} = 2Bm^{\text{phys}}$  and  $f$  as fit parameters in the constrained fits. Note that in this approach the low-energy constants  $\bar{\ell}_3$  and  $\bar{\ell}_4$  can still be determined, but they are no more independent, since they are linked to the LO constants as stated in equations (12, 13). The main purpose of this exercise is to show that our unconstrained fits did not need the additional degrees of freedoms to work, given that we used the pion mass and decay constants to set the scales for our lattice data. We performed fits with different mass ranges and limiting the lattice spacings included in our fits as before. In Fig. 13 we show the results for the fitted parameters and derived quantities as well as the  $\chi^2/\text{d.o.f.}$  for different mass ranges including only ensembles with  $1/a > 1.6 \text{ GeV}$ . The central values and error bands shown in these plots have been obtained as before: the central value and statistical error is the one from the fit with the mass range  $135 \text{ MeV} \leq M_{\pi} \leq 240 \text{ MeV}$ , while the systematic error has

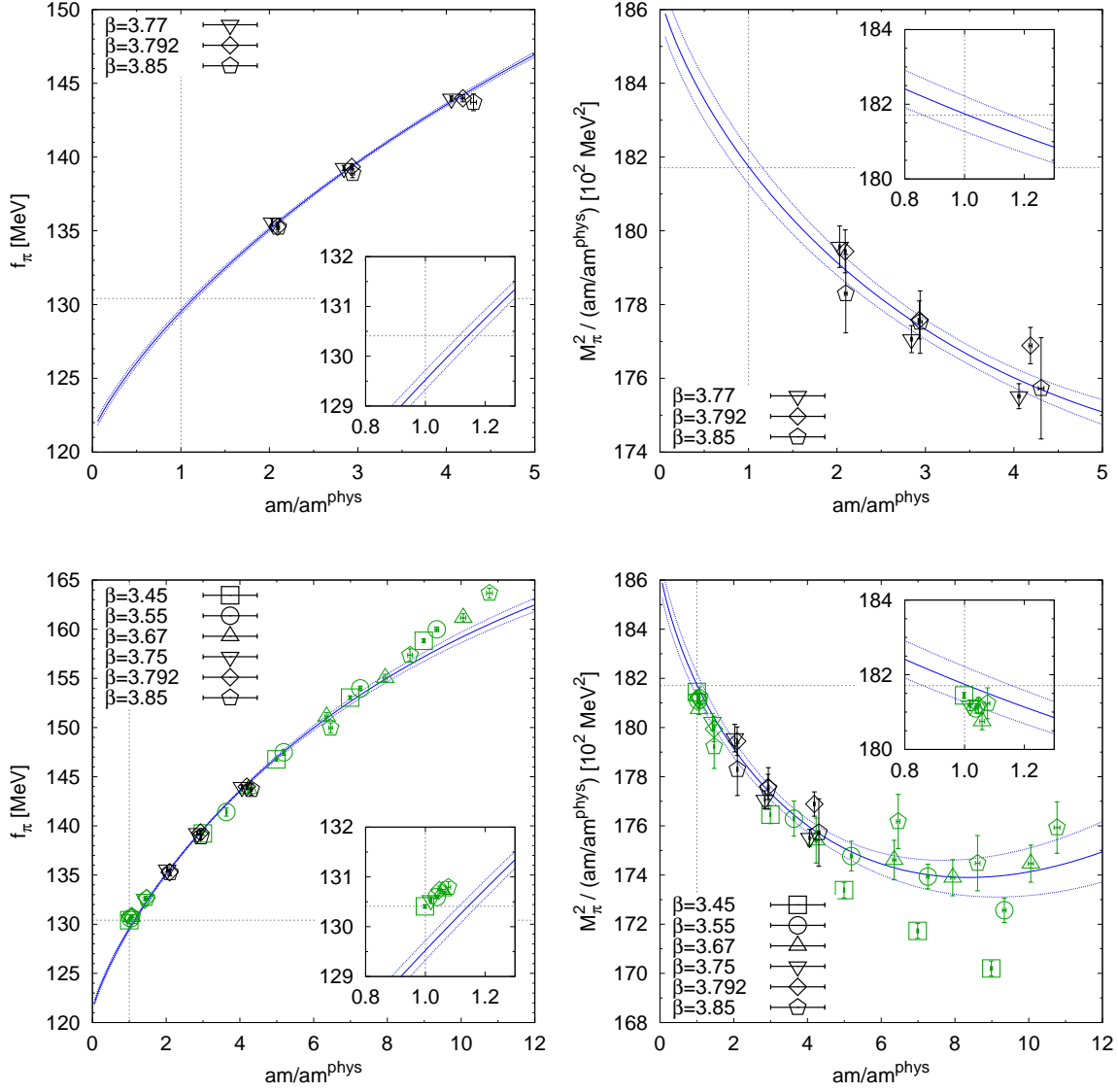


FIG. 11. Combined fit for lattice scales  $1/a > 1.6 \text{ GeV}$  and meson masses  $195 \text{ MeV} \leq M_\pi \leq 275 \text{ MeV}$  excluding the nearly physical points. *Left panels:* meson decay constant, *right panels:* squared meson mass divided by quark mass ratio. The *top panels* show only the points, which have been included in the fit, while the *bottom panels* show all points. There, points marked by *black symbols* are included in the fit, those marked by *green symbols* are excluded. The physical values are indicated by *dashed gray lines*.

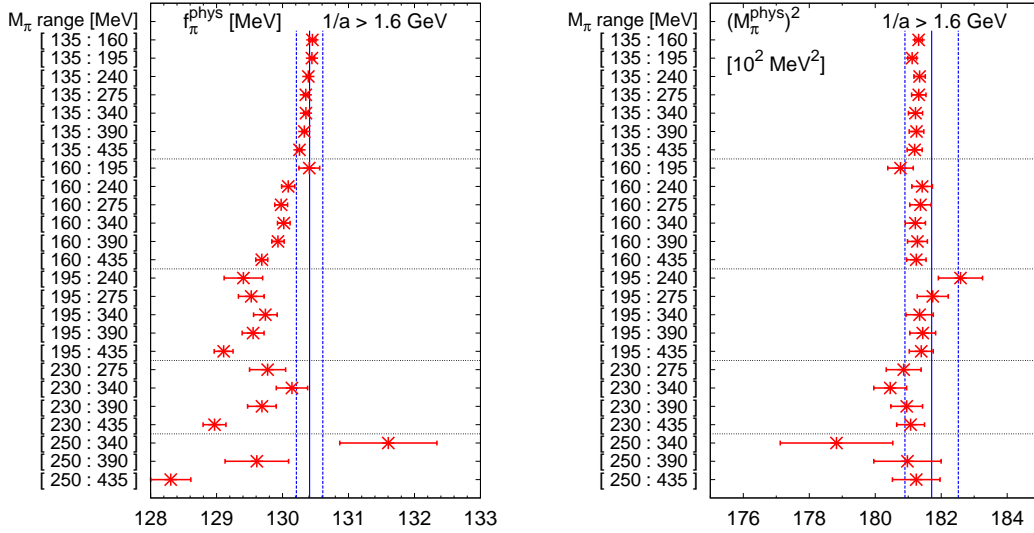


FIG. 12. Extrapolated  $f_\pi^{\text{phys}}$  (left panel) and  $(M_\pi^{\text{phys}})^2$  (right panel) from NLO ChPT fits without constraints using different mass ranges and including lattice spacings  $1/a > 1.6$  GeV. The *solid and dashed blue lines* denote the central value and total error bands, respectively as quoted by [19, 20].

been obtained from the variation with respect to the results from other fitting ranges in the meson mass. (We do not show the results from fits excluding the nearly physical points in this case, since due to the constraints these results now more or less agree with the results shown.) Figure 14 contains the plot showing the influence of the included lattice spacings on the fit results. We would like to state, that these parameter-reduced fits work equally well as the unconstrained ones, as measured by the resulting values for  $\chi^2/\text{d.o.f.}$ . Our estimates for the LECs and derived quantities from this fitting procedure are given in the right column of Tab. III (the first two parameters were fitted, the remaining ones were derived from these two). These values are in good agreement with the results from the unconstrained NLO-fits, given in the left column of that same table, but show a twice as large statistical and systematic error for  $\Lambda_3$  or equivalently  $\bar{\ell}_3$ , whereas the remaining uncertainties are roughly the same or slightly reduced.



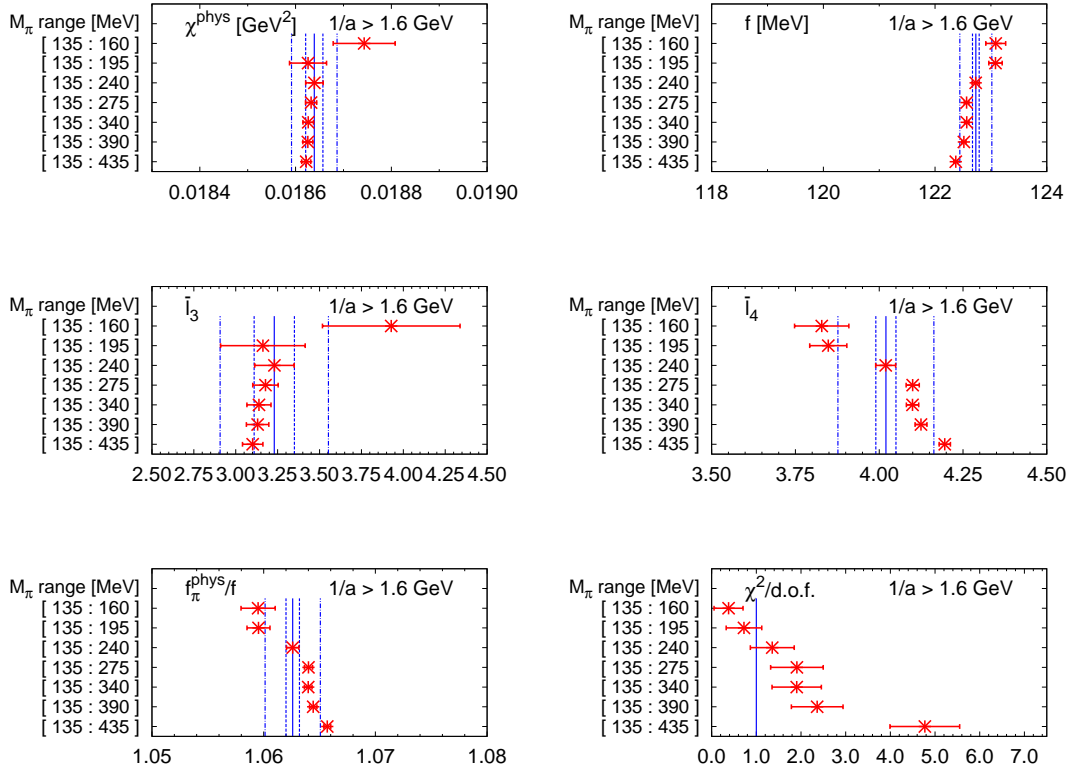


FIG. 13. Results for the fitted parameters (*top panels*) and  $\chi^2/\text{d.o.f}$  (*bottom right panel*) from parameter-reduced NLO ChPT fits using different mass ranges and including lattice spacings  $1/a > 1.6$  GeV. Also shown are the derived quantities  $\bar{l}_3$ ,  $\bar{l}_4$  (*middle panels*) and  $f_\pi^{\text{phys}}/f$  (*bottom left panel*). The *solid, dashed and dashed-dotted blue lines* for the fit parameters denote the central value, statistical and total (statistical plus systematic) error bands, respectively, from our preferred fit.

### C. Results for LECs

As our final set of low-energy constants determined from the NLO SU(2)-ChPT fits we quote the following values (which supersede the preliminary results in [7]).

$$\chi^{\text{phys}} = 2Bm^{\text{phys}} = 1.8609(18)_{\text{stat}}(74)_{\text{sys}} \cdot 10^{-2} \text{ GeV}^2, \quad (16)$$

$$f = 122.72(07)_{\text{stat}}(35)_{\text{sys}} \text{ MeV}, \quad (17)$$

$$\Lambda_3 = 653(32)_{\text{stat}}(101)_{\text{sys}} \text{ MeV}, \quad (18)$$

$$\Lambda_4 = 1,009(16)_{\text{stat}}(77)_{\text{sys}} \text{ MeV}, \quad (19)$$

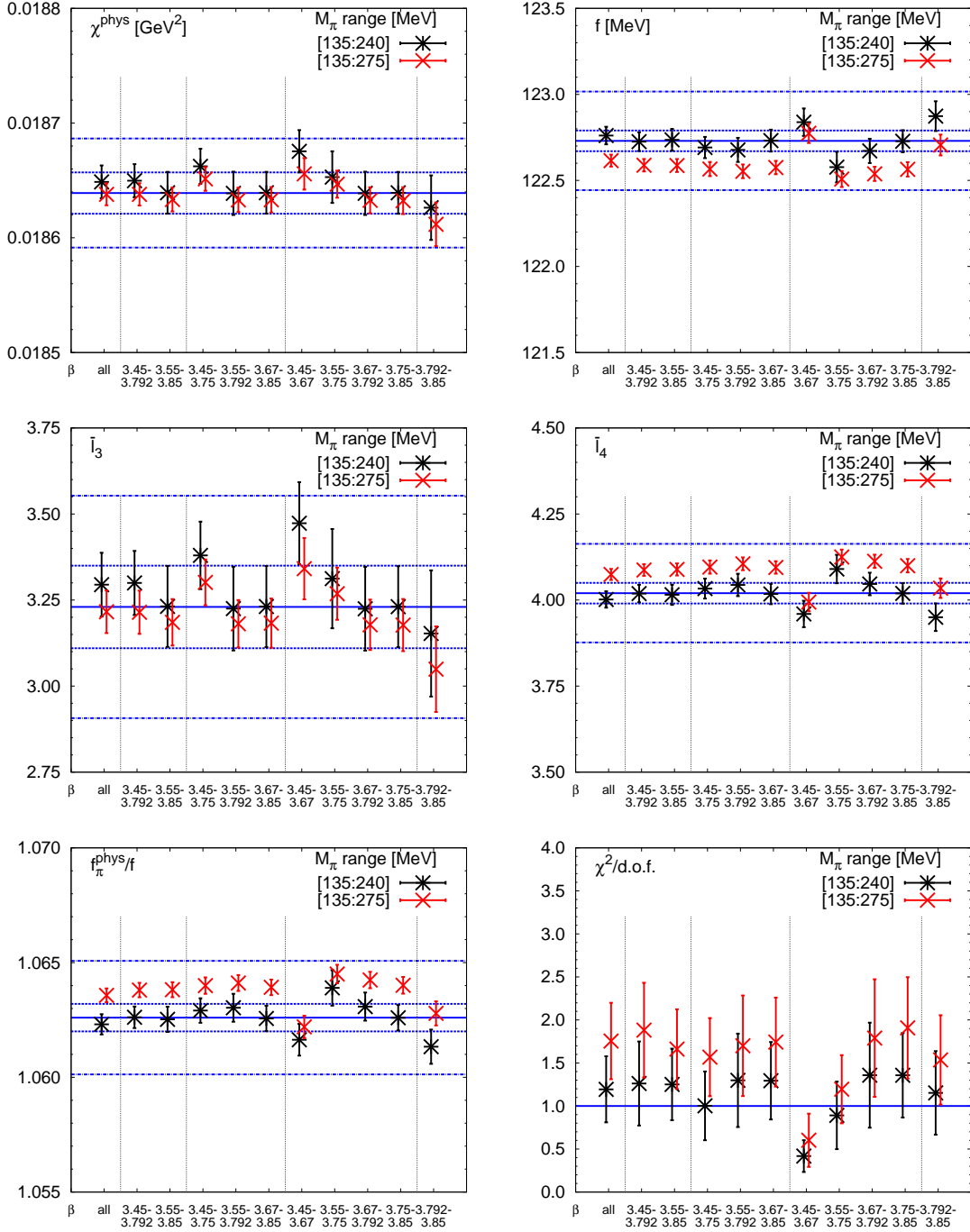


FIG. 14. Fit parameters and  $\chi^2/\text{d.o.f.}$  from parameter-reduced NLO ChPT fits to two different mass ranges, where several lattice spacings have been excluded. *Vertical dashed lines* group points where no, one, two, three or four (from left to right) lattice spacings have been excluded. The *solid, dashed and dashed-dotted horizontal blue lines* denote the central value, statistical and total (statistical plus systematic) error bands, respectively, from our preferred fit.

$$\bar{\ell}_3 = 3.16(10)_{\text{stat}}(29)_{\text{syst}} , \quad (20)$$

$$\bar{\ell}_4 = 4.03(03)_{\text{stat}}(16)_{\text{syst}} , \quad (21)$$

$$f_\pi^{\text{phys}}/f = 1.0627(06)_{\text{stat}}(27)_{\text{syst}} . \quad (22)$$

Here we averaged the central values and statistical uncertainties from the unconstrained (Sec. IV B 1) and parameter-reduced (Sec. IV B 2) fits (both summarized in Tab. III). For the square of the systematic uncertainty we sum the squares of the average systematic uncertainty and of the spread of the central values.

## V. FITS TO NNLO-SU(2) CHPT

As a further step, we examined the effects of fitting our data to SU(2)-ChPT including terms up to next-to-next-to-leading order (NNLO). The motivation for this exercise is two-fold. On the one hand, we would like to check whether or not our results obtained for the LECs by fitting to NLO-ChPT are stable when considering the next higher order in ChPT. On the other hand, there is some general interest in whether the amount of data is sufficient to reliably determine the additional fit parameters appearing at NNLO and whether NNLO-ChPT is superior to NLO-ChPT in terms of describing the data (as measured, e.g., by the  $\chi^2/\text{d.o.f.}$ ).

### A. Fit formulae

The formulae for the squared meson mass and the meson decay constant up to NNLO read (cf. [19, 25])

$$M_\pi^2 = \chi \left[ 1 + \frac{\chi}{16\pi^2 f^2} \log \frac{\chi}{\Lambda_3^2} + \text{NNLO}_{M^2} \right] , \quad (23)$$

$$f_\pi = f \left[ 1 - \frac{\chi}{8\pi^2 f^2} \log \frac{\chi}{\Lambda_4^2} + \text{NNLO}_f \right] , \quad (24)$$

$$\text{NNLO}_{M^2} = \left( \frac{\chi l}{16\pi^2 f^2} \right)^2 \left[ \frac{1}{306} \left( 60 \log \frac{\chi}{\Lambda_{12}^2} - 9 \log \frac{\chi}{\Lambda_3^2} - 49 \right)^2 + 4k_{M^2} \right] , \quad (25)$$

$$\text{NNLO}_f = \left( \frac{\chi l}{16\pi^2 f^2} \right)^2 \left[ -\frac{1}{180} \left( 30 \log \frac{\chi}{\Lambda_{12}^2} + 6 \log \frac{\chi}{\Lambda_3^2} - 6 \log \frac{\chi}{\Lambda_4^2} - 23 \right)^2 + 4k_f \right] . \quad (26)$$

Up to this order three new fit parameters enter: one additional low energy scale  $\Lambda_{12}$  and the two NNLO-LECs  $k_{M^2}$ ,  $k_f$ . The low energy scale  $\Lambda_{12}$  is related to the low energy scales usually denoted by  $\Lambda_1$  and  $\Lambda_2$  in the literature via

$$\log \Lambda_{12}^2 = \frac{7}{15} \log \Lambda_1^2 + \frac{8}{15} \log \Lambda_2^2. \quad (27)$$

The low energy scales  $\Lambda_1$ ,  $\Lambda_2$  already appear separately in the NLO-formulae for other quantities (e.g. scattering lengths in  $\pi\pi$ -scattering [25]), but since in our case only the combination  $\Lambda_{12}$  appears, we will not be able to distinguish between them. As before, the low-energy scales can also be expressed via the LECs  $\bar{\ell}_i$  as in Eq. (10), i.e.

$$\bar{\ell}_i = \log \frac{\Lambda_i^2}{(M_\pi^{\text{phys}})^2}, \quad i = 1, 2, 3, 4, 12. \quad (28)$$

## B. Combined global fits

We applied the same fit strategy for the NNLO-fits as for the NLO-fits (see previous section): the scale and light quark mass at the physical point as determined in Sec. III are used and combined global fits to our data for the meson masses and decay constants are performed. First, we will discuss fits without any assumptions on the fit parameters (Sec. VB 1). Later we will also constrain the additional fit parameters entering at NNLO by phenomenologically motivated estimates (Sec. VB 2).

### 1. NNLO fits without priors

We will start our discussion with fit ranges including the nearly physical points and only consider varying the upper mass limit of the fit range. Since now three more parameters have to be determined, it can be expected that we will have to include more data-points, i.e., including higher meson masses, compared to the NLO-case. Indeed, with too few data-points either the fitter could not find a solution at all or some of the fitted parameters had big numerical uncertainties. This can be seen in the compilation in Fig. 15 of fit results using ensembles with  $1/a > 1.6$  GeV, e.g., for the fit ranges  $135 \text{ MeV} \leq M_\pi \leq 240 \text{ MeV}$ ,  $135 \text{ MeV} \leq M_\pi \leq 275 \text{ MeV}$  and maybe also  $135 \text{ MeV} \leq M_\pi \leq 340 \text{ MeV}$ .

The plots of a sample fit with the range  $135 \text{ MeV} \leq M_\pi \leq 390 \text{ MeV}$ ,  $1/a > 1.6$  GeV are given in Fig. 16 (only data points included in the fit range are shown in these plots).

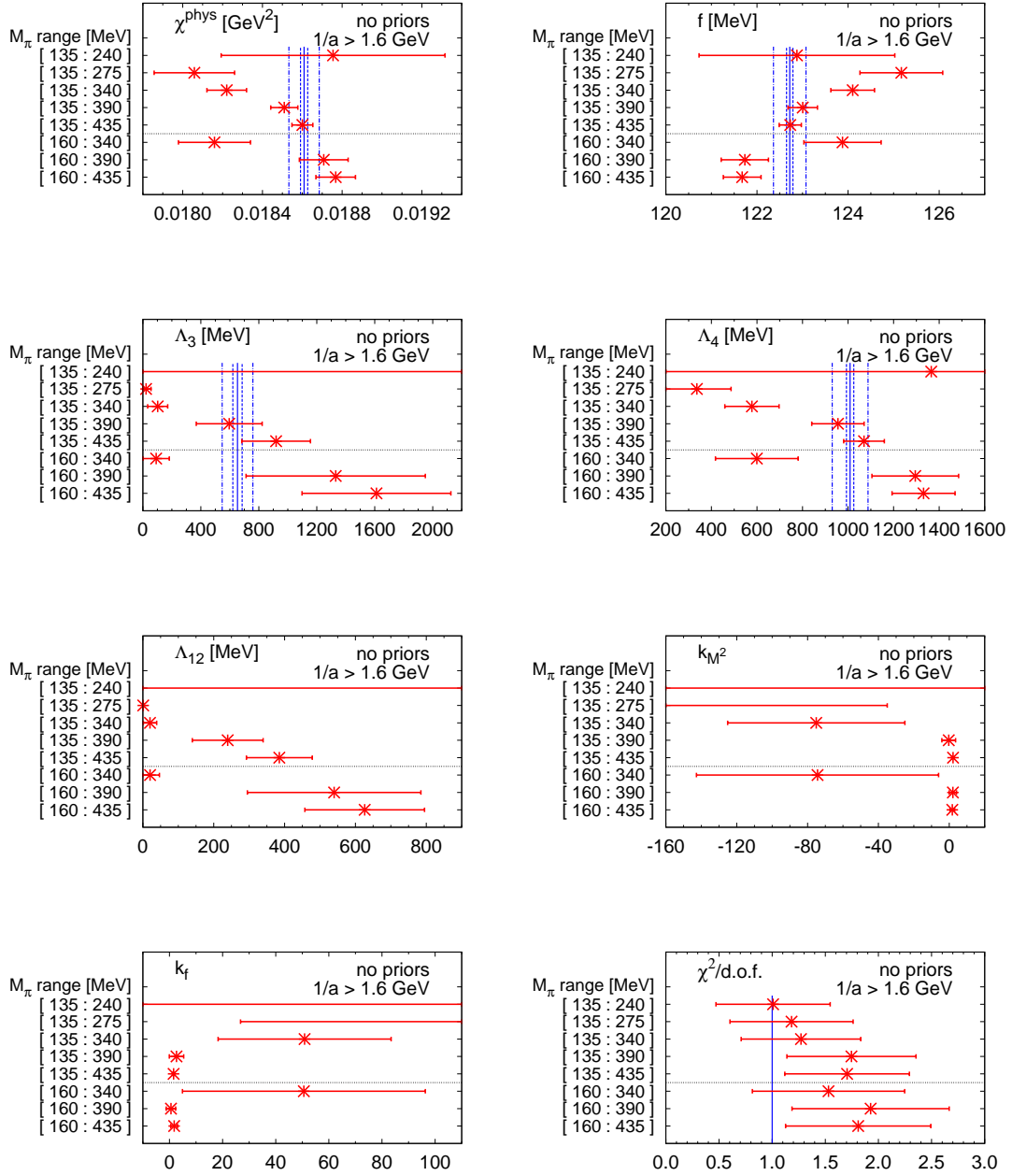


FIG. 15. Results for the fitted parameters and  $\chi^2/\text{d.o.f}$  from NNLO ChPT fits without constraints using different mass ranges and including lattice spacings  $1/a > 1.6 \text{ GeV}$ . The *solid*, *dashed* and *dashed-dotted blue lines* for the fit parameters denote the central value, statistical and total (statistical plus systematic) error bands, respectively, from our NLO-fits.

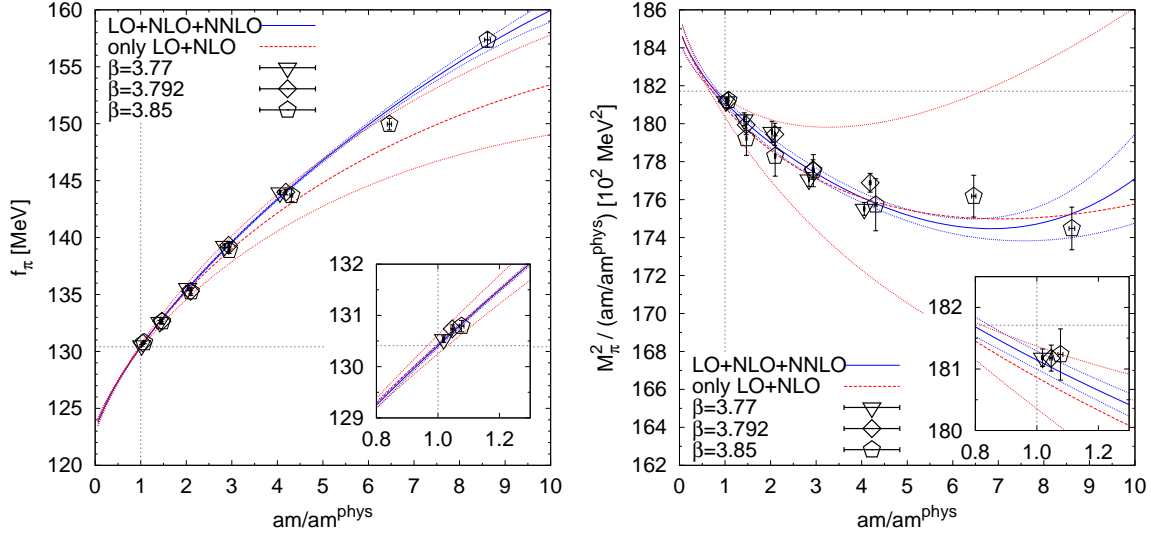


FIG. 16. Combined NNLO-fit for lattice scales  $1/a > 1.6 \text{ GeV}$  and meson masses  $135 \text{ MeV} \leq M_\pi \leq 390 \text{ MeV}$ . *Left panel*: meson decay constant, *right panel*: squared meson mass divided by quark mass ratio. The *solid blue lines* show the complete (up to NNLO) fit, whereas the *dashed red lines* show the LO+NLO contribution of the full NNLO-fit. Only data points included in the fit range are depicted in the plots, the physical values are marked by *dashed gray lines*.

Although technically the fit seems to work well resulting in an acceptable  $\chi^2/\text{d.o.f.} = 1.8(0.6)$  one should take the result *cum grano salis*. Besides the fitted curve up to NNLO (solid blue line with error band indicated by blue dotted lines), each plot also shows the LO+NLO contribution separately (dashed red line with error band indicated by red dotted lines), i.e., the NNLO contribution being the difference between the solid blue and the dashed red line. In this case, the NLO- and NNLO-contributions taken separately seem to have big uncertainties. In other cases, we found the NNLO-contribution to have an unnaturally large effect even at small quark masses.

At this point, we have to conclude that NNLO-fits to our current data are not convincing for the reasons outlined above. This situation might improve, once more data points in the region between the physical point (or below) and, say, 200 MeV or 250 MeV will be added to the analysis, allowing for fits using a smaller mass range (like we were able to do for the NLO-fits). Since the generation of such data points is not planned for the near future, we will in the remainder of this section examine whether constraining the additional NNLO fit

parameters can serve as a remedy to this situation (and which side-effects this remedy has).

## 2. NNLO fits using priors

To stabilize the NNLO fits, we examined the effect of using priors for the three additional fit parameters  $\Lambda_{12}$ ,  $k_{M^2}$ , and  $k_f$ . Since we are mainly interested to learn how the parameters already appearing at NLO change, when going from NLO to NNLO fits, we did not consider adding priors for these parameters as well.

The priors were implemented in the fitting procedure via an augmented  $\chi^2$ . Instead of minimizing the usual  $\chi^2$  (sum of deviations of the data points from the fitted function weighted by the uncertainty of that data point) the modified

$$\chi_{\text{augmented}}^2 = \chi^2 + \sum_n \frac{(p_n - p_n^{\text{prior}})^2}{(\sigma_n^{\text{prior}})^2} \quad (29)$$

is minimized by the fitting routine. Here  $n$  runs over all fit parameters  $p_n$  to which a prior  $p_n^{\text{prior}}$  with width  $\sigma_n^{\text{prior}}$  has been assigned. That is, the fitting routine ‘‘punishes’’ a parameter for leaving the prior interval  $p_n^{\text{prior}} \pm \sigma_n^{\text{prior}}$ .

In the following we will use either a prior for  $\bar{\ell}_{12}$  alone or together with priors for  $k_{M^2}$  and  $k_f$ . We will assign the following values for the priors to the fit parameters:

$$\bar{\ell}_{12}^{\text{prior}} = 2.1 \pm 0.3 \quad (30)$$

$$k_{M^2}^{\text{prior}} = 0 \pm 10 \quad (31)$$

$$k_f^{\text{prior}} = 0 \pm 10 \quad (32)$$

The prior for  $\bar{\ell}_{12}$  has been obtained from the estimates for the LECs  $\bar{\ell}_1 = -0.4 \pm 0.6$  and  $\bar{\ell}_2 = 4.3 \pm 0.1$  extracted from  $\pi\pi$ -scattering data in [25] via

$$\bar{\ell}_{12}^{\text{prior}} = \frac{7}{15} \bar{\ell}_1^{\text{prior}} + \frac{8}{15} \bar{\ell}_2^{\text{prior}}$$

cf. Eqs. (27) and (28). This would translate into a prior for the low energy scale

$$\Lambda_{12}^{\text{prior}} = 385 \text{ MeV} \pm 58 \text{ MeV}. \quad (33)$$

The priors for the NNLO-LECs  $k_{M^2}$  and  $k_f$  are merely based on assuming a natural order of magnitude for these corrections. We are aware that the latter is a rather weak argument, for that reason we did not use the priors on  $k_{M^2}$  and  $k_f$  alone and results from fits using

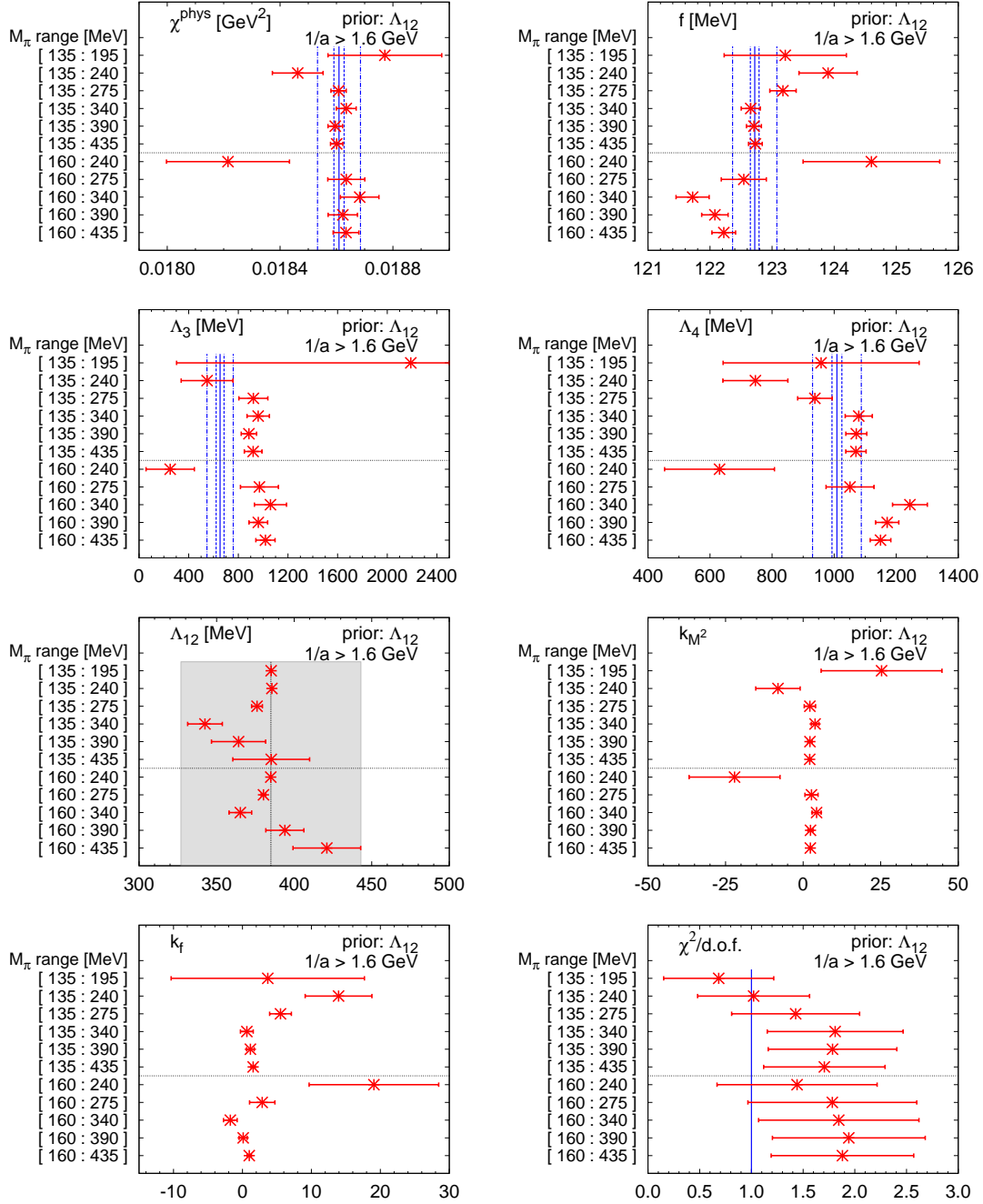


FIG. 17. Results for the fitted parameters and  $\chi^2/\text{d.o.f}$  from NNLO ChPT fits with a prior for  $\Lambda_{12}$  using different mass ranges and including lattice spacings  $1/a > 1.6 \text{ GeV}$ . The *solid*, *dashed* and *dashed-dotted blue lines* for the fit parameters denote the central value, statistical and total (statistical plus systematic) error bands, respectively, from our NLO-fits. The used prior and its width is indicated by the *dashed black line* and the *shaded grey area*, respectively.



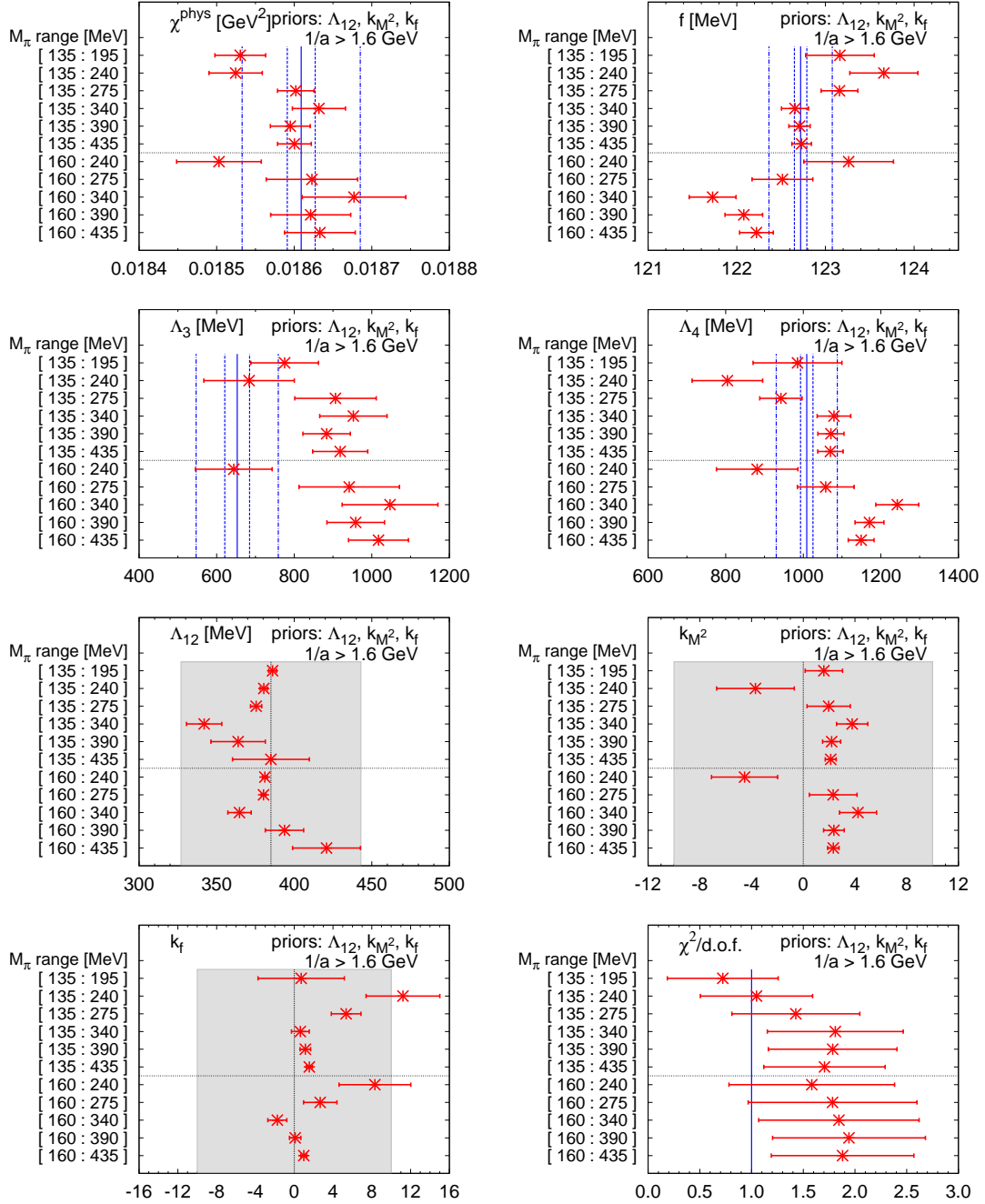


FIG. 18. Results for the fitted parameters and  $\chi^2/\text{d.o.f}$  from NNLO ChPT fits with priors for  $\Lambda_{12}$ ,  $k_{M^2}$ , and  $k_f$  using different mass ranges and including lattice spacings  $1/a > 1.6$  GeV. The *solid, dashed and dashed-dotted blue lines* for the fit parameters denote the central value, statistical and total (statistical plus systematic) error bands, respectively, from our NLO-fits. The used priors and their widths are indicated by the *dashed black lines* and the *shaded grey areas*, respectively.

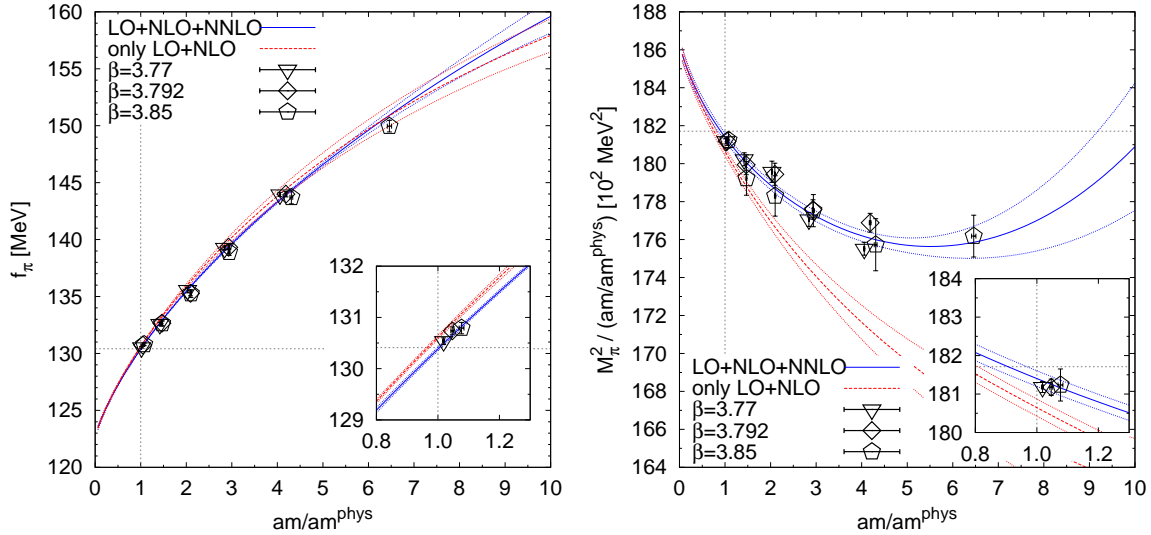


FIG. 19. Combined NNLO-fit for lattice scales  $1/a > 1.6 \text{ GeV}$  and meson masses  $135 \text{ MeV} \leq M_\pi \leq 340 \text{ MeV}$  using a prior for  $\Lambda_{12}$ . *Left panel*: meson decay constant, *right panel*: squared meson mass divided by quark mass ratio. The *solid blue lines* show the complete (up to NNLO) fit, whereas the *dashed red lines* show the LO+NLO contribution of the full NNLO-fit. Only data points included in the fit range are depicted in the plots, the physical values are marked by *dashed gray lines*.

these priors should be taken with some caution. However, these priors are to some extent justified by the NNLO fits where no priors have been used (see Fig. 15) and also, as we will see, by fits where only the prior on  $\bar{\ell}_{12}$  has been used.

The results from the fits to different mass ranges using priors on  $\bar{\ell}_{12}$  only or on  $k_{M^2}$  and  $k_f$  as well are shown in Figs. 17 and 18, respectively, where only the ensembles with  $1/a > 1.6 \text{ GeV}$  have been used. The used priors are indicated by the gray shaded areas. As an effect, now fits to smaller mass ranges are possible and/or are more stable judging from the uncertainties of the fit parameters. In Figs. 19 and 20 we show as examples the fits for the mass range  $135 \text{ MeV} \leq M_\pi \leq 340 \text{ MeV}$ . Whereas in both cases for the decay constant the NNLO-contribution seems to be reasonable small, for the meson mass the NNLO-contribution is more substantial. Nevertheless, the error bands for the LO+NLO contribution are now reasonable as well, showing again the stabilizing effect of using the priors.

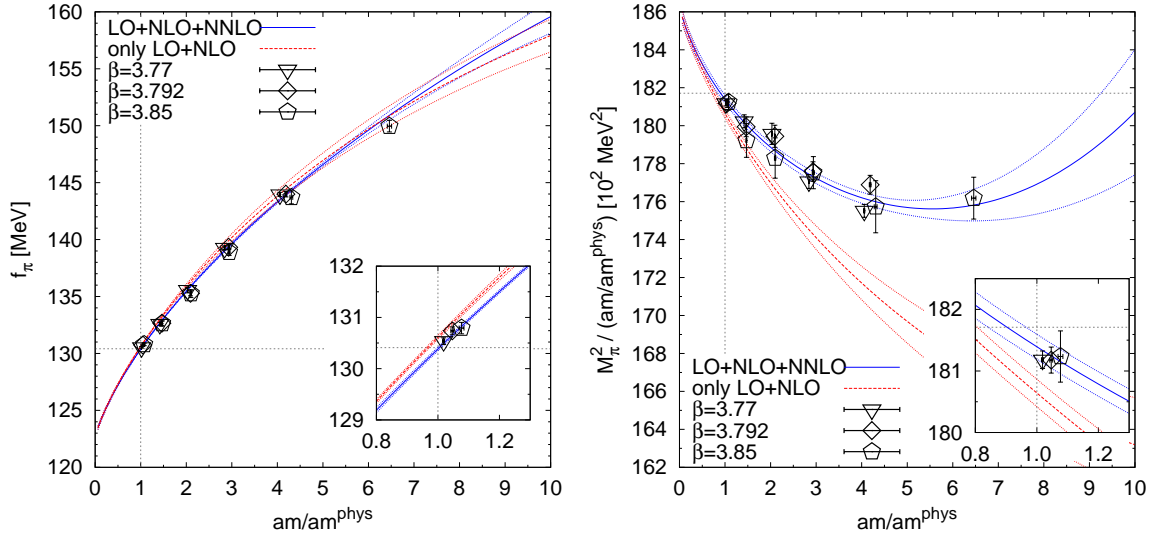


FIG. 20. Combined NNLO-fit for lattice scales  $1/a > 1.6 \text{ GeV}$  and meson masses  $135 \text{ MeV} \leq M_\pi \leq 340 \text{ MeV}$  using priors for  $\Lambda_{12}$ ,  $k_{M^2}$ , and  $k_f$ . *Left panel:* meson decay constant, *right panel:* squared meson mass divided by quark mass ratio. The *solid blue lines* show the complete (up to NNLO) fit, whereas the *dashed red lines* show the LO+NLO contribution of the full NNLO-fit. Only data points included in the fit range are depicted in the plots, the physical values are marked by *dashed gray lines*.

In Figs. 21 and 22 we compare the LECs and the ratio  $f_\pi^{\text{phys}}/f$  from the NNLO fits to different mass ranges using either no priors or one of our choices for the set of priors (all for ensembles with  $1/a > 1.6 \text{ GeV}$ ). Our final results with total error bands from the NLO-fits are always indicated by the blue lines. In the case of  $\bar{\ell}_3$ , the fits using priors shift the value of the LECs a bit upward, whereas  $\bar{\ell}_4$  and  $f_\pi^{\text{phys}}/f$  just fluctuate within the total error band from the NLO-fit. The comparison for the LEC  $\bar{\ell}_{12}$  again demonstrates the stabilizing effect of the priors or—in the other words—the difficulties we encountered in the fits without using priors. In the latter case (top right panel of Fig. 22), the fit result only comes close to the phenomenological estimate, Eq. (30), for fit ranges including meson masses of 390 MeV or higher.

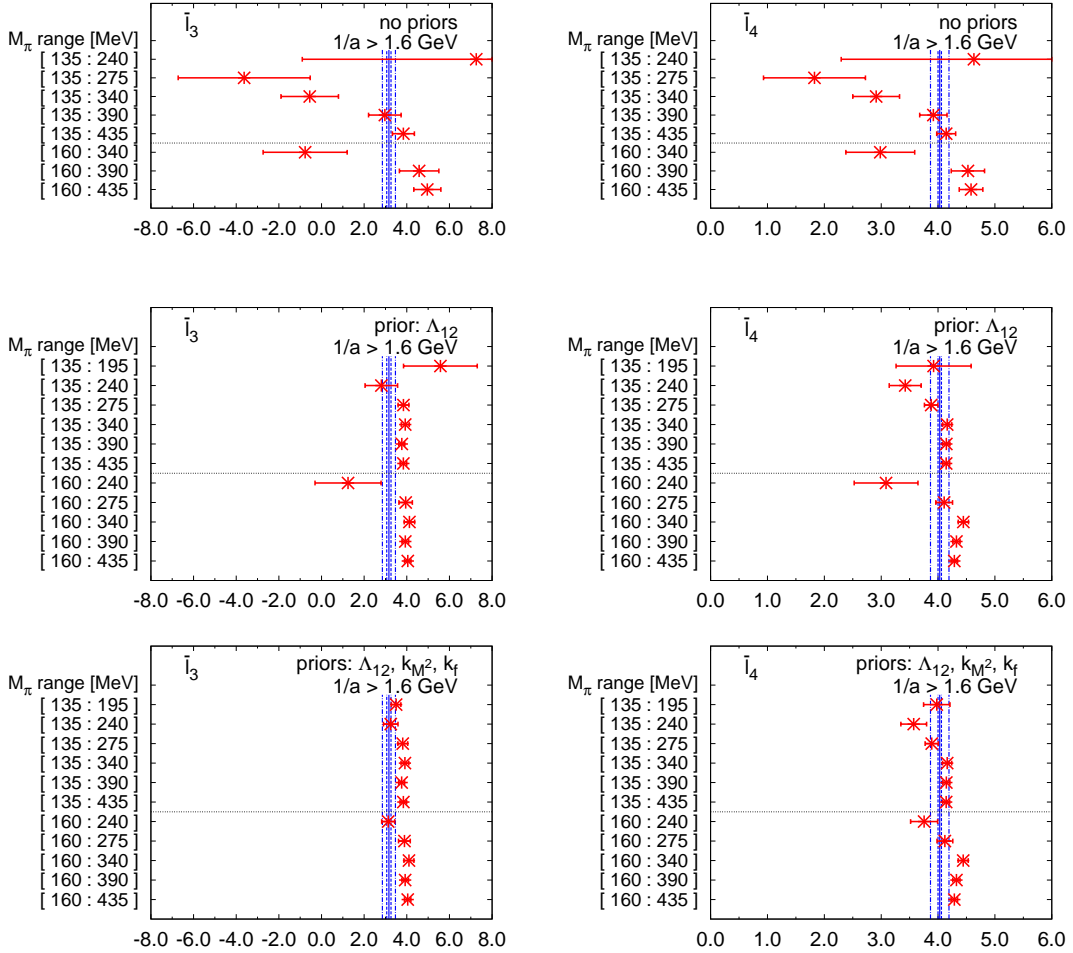


FIG. 21. Results for the LECs  $\bar{\ell}_3$  (left panels) and  $\bar{\ell}_4$  (right panels) from NNLO fits to ensembles with  $1/a > 1.6 \text{ GeV}$  and different mass ranges. The top, middle, and bottom panels show the results using no priors, a prior for  $\Lambda_{12}$ , and priors for  $\Lambda_{12}$ ,  $k_{M^2}$ , and  $k_f$ , respectively. The solid, dashed, and dashed dotted blue lines indicate the central value, statistical and total (statistical plus systematic) error bands from our NLO-fits.

## VI. CONCLUSIONS

In this paper we presented a determination of the NLO low-energy constants  $\bar{\ell}_3$  and  $\bar{\ell}_4$  of SU(2) chiral perturbation theory from 2+1 flavor lattice simulations with staggered fermions. In addition we gave results for the LO quantities  $f$  (or  $f_\pi^{\text{phys}}/f$ ) and  $B$  (or  $\chi^{\text{phys}} = Bm^{\text{phys}}$ ). The quantities  $\bar{\ell}_{3,4}$  are also expressed in terms of the scales  $\Lambda_{3,4}$ , respectively.

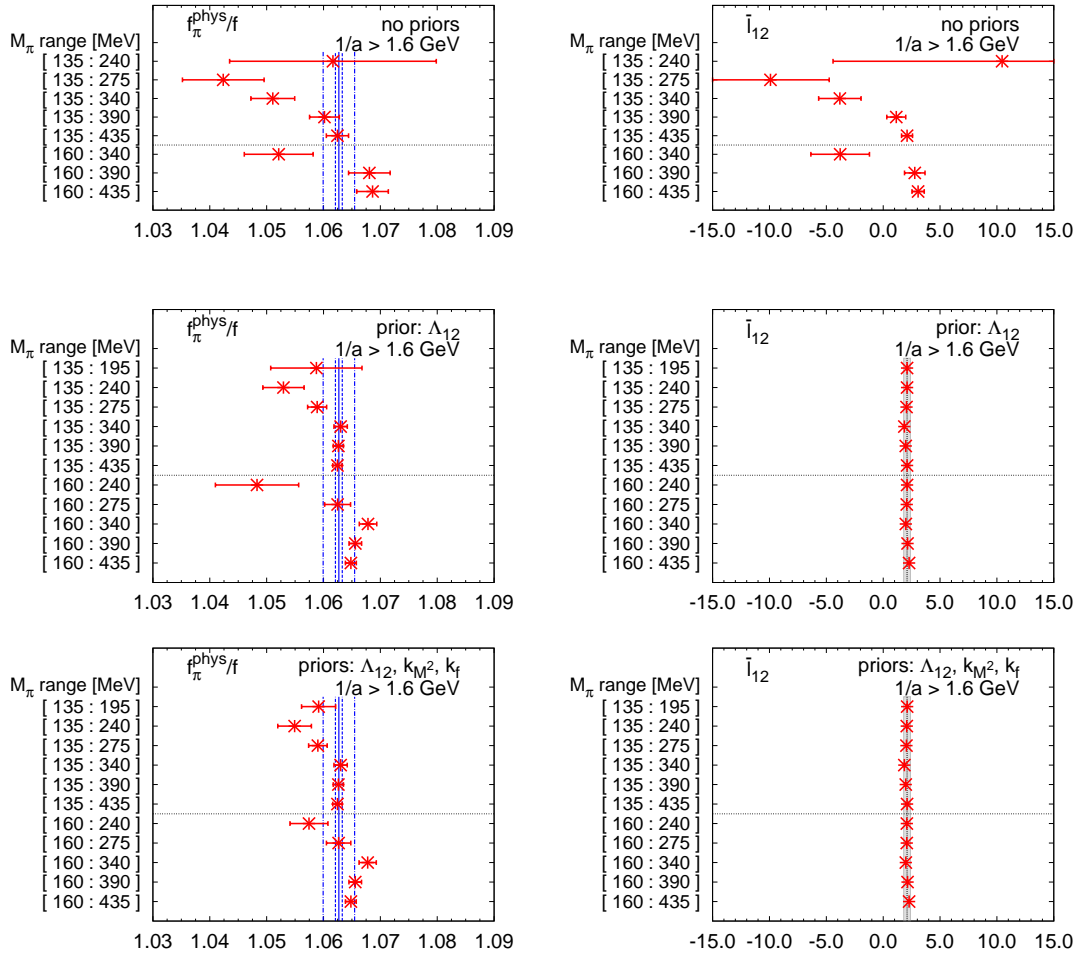


FIG. 22. Results for the ratio  $f_{\pi}^{\text{phys}}/f$  (left panels) and the LEC  $\bar{\ell}_{12}$  (right panels) from NNLO fits to ensembles with  $1/a > 1.6$  GeV and different mass ranges. The *top*, *middle*, and *bottom* panels show the results using no priors, a prior for  $\Lambda_{12}$ , and priors for  $\Lambda_{12}$ ,  $k_M^2$ , and  $k_f$ , respectively. The *solid*, *dashed*, and *dashed dotted blue* lines indicate the central value, statistical and total (statistical plus systematic) error bands from our NLO-fits. The *dashed black* lines and *grey shaded areas* indicate the used prior and its width (where applicable).

Our final results as presented in equations (16-22) stem from fits which use the NLO functional form. The result for  $\chi^{\text{phys}}$  amounts to a condensate parameter

$$B(2 \text{ GeV}) = 2.682(36)(39) \text{ GeV} \quad (34)$$

if one divides out the value of the average light quark mass from Ref. [26, 27]. Moreover,

after multiplying with  $F^2 = f^2/2$  from (17) one obtains

$$\Sigma(2 \text{ GeV}) = 2.020(27)(31) 10^{-2} \text{ GeV}^3 \quad \text{or} \quad \Sigma(2 \text{ GeV})^{1/3} = 0.2723(12)(14) \text{ GeV} \quad (35)$$

where all quantities given at the scale  $\mu = 2 \text{ GeV}$  refer to the  $\overline{\text{MS}}$  scheme. These results are reasonably consistent with the high-quality entries in Table 10 of Ref. [19], in particular with those by the MILC [17], RBC/UKQCD [28], and ETM [29] collaborations, to mention some of the most precise determinations. Similarly, our results

$$\bar{\ell}_3 = 3.16(10)(29) \quad \text{and} \quad \bar{\ell}_4 = 4.03(03)(16)$$

as stated in (20) and (21), respectively, are in good agreement with the broad majority of the entries in Table 12 of Ref. [19], in particular with those by the MILC [30], RBC/UKQCD [28], and ETM [29] collaborations. Finally, our result (22) for the ratio  $f_\pi^{\text{phys}}/f$  agrees with the entries of Table 11 in of Ref. [19], perhaps with some slight tension when compared to the recent 2+1+1 flavor result by the ETM collaboration [31].

We have carefully examined the effect of various cuts on the data, in particular the effect of requesting  $a^{-1} > 1.6 \text{ GeV}$  and the effect of limiting the pion mass range that enters the chiral fit. It turns out that the restriction to fine lattices improves the quality of the fits, and with this restriction reasonably stable NLO results are obtained for pion mass windows up to  $\sim 400 \text{ MeV}$ . Given the fine grained set of pion masses available in our ensemble basis, we can even explore the effect of dropping some of the lighter data points. We find that  $\bar{\ell}_3$  is much more robust in this respect than  $\bar{\ell}_4$  (or  $f_\pi^{\text{phys}}/f$ ), as is evident from Fig. 9.

Finally, we have explored the effect of adding the NNLO contribution to the functional ansatz. To prevent a dramatic increase of the number of free parameters we add priors for the new NLO combinations (in which we are not interested) and the genuine NNLO coefficients (to which our data show little sensitivity). We find it very reassuring that these prior-aided NNLO fits remain stable (for a reasonable range of lattice spacings and pion mass windows), and that the resulting fits show a very natural ordering between LO, NLO, and NNLO contributions (out to  $M_\pi \sim 400 \text{ MeV}$ ). Moreover, the NLO coefficients  $\bar{\ell}_3$  and  $\bar{\ell}_4$  as determined from these prior-aided NNLO fits are in good agreement with the results of the direct NLO fits. We take this as a sign that our assessment of the systematic uncertainties of these quantities is true and fair.

As stated in Section IV we did not attempt to include terms designed to absorb cut-off effects into our formulas. The purpose of the present work was to explore whether such

terms are mandatory; we find that they are not (with the level of precision of our data), albeit at the price of pruning the dataset to include only lattices with  $a^{-1} > 1.6 \text{ GeV}$ . It remains open to which extent it would prove helpful to include such cut-off terms; we may address this point in a future study.

In summary, our results (16-22) and (34,35) indicate that SU(2) chiral low-energy constants can be determined on the lattice with a precision at the level of a few percent for the LO quantities  $B$ ,  $\Sigma$ ,  $f$ , and the level of  $O(10\%)$  for the NLO scales  $\Lambda_3$ ,  $\Lambda_4$ .

### ACKNOWLEDGMENTS

Computations were performed using HPC resources from FZ Jülich and on clusters at Wuppertal University. This work is supported in part by EU Grants PITN-GA-2009-238353 (ITN STRONGnet), PIRG07-GA-2010-268367, DFG Grant No. FO 502/2 and SFB-TR 55.

- 
- [1] H. Fritzsch, M. Gell-Mann, and H. Leutwyler, *Phys.Lett.* **B47**, 365 (1973).
  - [2] J. Gasser and H. Leutwyler, *Annals Phys.* **158**, 142 (1984).
  - [3] J. Gasser and H. Leutwyler, *Nucl.Phys.* **B250**, 465 (1985).
  - [4] K. G. Wilson, *Phys.Rev.* **D10**, 2445 (1974).
  - [5] M. Creutz, *Phys.Rev.* **D21**, 2308 (1980).
  - [6] S. Dürr *et al.*, *Science* **322**, 1224 (2008), arXiv:0906.3599.
  - [7] E. E. Scholz *et al.*, *PoS LATTICE2011*, 142 (2011), arXiv:1111.3729.
  - [8] M. Lüscher and P. Weisz, *Phys.Lett.* **B158**, 250 (1985).
  - [9] C. Morningstar and M. J. Peardon, *Phys.Rev.* **D69**, 054501 (2004), arXiv:hep-lat/0311018.
  - [10] Y. Aoki *et al.*, *JHEP* **0601**, 089 (2006), arXiv:hep-lat/0510084.
  - [11] S. Dürr *et al.*, *Phys.Rev.* **D79**, 014501 (2009), arXiv:0802.2706.
  - [12] Y. Aoki *et al.*, *Phys.Lett.* **B643**, 46 (2006), arXiv:hep-lat/0609068.
  - [13] Y. Aoki *et al.*, *Nature* **443**, 675 (2006), arXiv:hep-lat/0611014.
  - [14] Y. Aoki *et al.*, *JHEP* **0906**, 088 (2009), arXiv:0903.4155.
  - [15] S. Borsanyi *et al.*, *JHEP* **1009**, 073 (2010), arXiv:1005.3508.
  - [16] S. Borsanyi *et al.*, *JHEP* **1011**, 077 (2010), arXiv:1007.2580.

- [17] A. Bazavov *et al.*, Rev.Mod.Phys. **82**, 1349 (2010), arXiv:0903.3598.
- [18] G. Colangelo, S. Dürr, and C. Haefeli, Nucl.Phys. **B721**, 136 (2005), arXiv:hep-lat/0503014.
- [19] G. Colangelo *et al.*, Eur.Phys.J. **C71**, 1695 (2011), arXiv:1011.4408.
- [20] Particle Data Group, K. Nakamura *et al.*, J.Phys.G **G37**, 075021 (2010).
- [21] C. Aubin and C. Bernard, Phys. Rev. **D68**, 034014 (2003), arXiv:hep-lat/0304014.
- [22] C. Aubin and C. Bernard, Phys. Rev. **D68**, 074011 (2003), arXiv:hep-lat/0306026.
- [23] T. Blum *et al.*, Phys.Rev. **D55**, 1133 (1997), arXiv:hep-lat/9609036.
- [24] MILC Collaboration, K. Orginos, D. Toussaint, and R. Sugar, Phys.Rev. **D60**, 054503 (1999), arXiv:hep-lat/9903032.
- [25] G. Colangelo, J. Gasser, and H. Leutwyler, Nucl.Phys. **B603**, 125 (2001), arXiv:hep-ph/0103088.
- [26] S. Dürr *et al.*, Phys.Lett. **B701**, 265 (2011), arXiv:1011.2403.
- [27] S. Dürr *et al.*, JHEP **1108**, 148 (2011), arXiv:1011.2711.
- [28] RBC/UKQCD Collaborations, Y. Aoki *et al.*, Phys.Rev. **D83**, 074508 (2011), arXiv:1011.0892.
- [29] ETM Collaboration, R. Baron *et al.*, JHEP **1008**, 097 (2010), arXiv:0911.5061.
- [30] A. Bazavov *et al.*, PoS **LATTICE2010**, 083 (2010), arXiv:1011.1792.
- [31] R. Baron *et al.*, JHEP **1006**, 111 (2010), arXiv:1004.5284.